Publication No. U-3637

FINAL REPORT

ANALYSIS OF PERTURBATION SOLUTIONS OF VARIED THRUST TRAJECTORIES

Prepared for: National Aeronautics and Space Administration
George C. Marshall Space Flight Center
Huntsville, Alabama

Under Contract: NAS8-20150

Prepared by: Richard R. Auelmann
Phillip T. Lane

27 June 1966

AERONUTRONIC
DIVISION OF PHILCO CORPORATION
A SUBSIDIARY OF Ford Motor Company
FORD ROAD/NEWPORT BEACH, CALIFORNIA

CONTENTS

SECTION		PAGE
1	INTRODUCTION AND SUMMARY	1
2	INTERPLANETARY TRANSFER	5
	2.1 The Energy Momentum Diagram	5
	2.2 The Powered Thrust Segments	5
	2.3 Solutions Using Tangential Thrust Acceleration	11
	2.4 Review of Optimal Solutions for Restricted Flight Times	14
	2.5 Analytic Solutions for Constant Steering Angles	20
3	APPROXIMATE ANALYTIC SOLUTIONS FOR PLANETARY ESCAPE AND CAPTURE	30
	3.1 Introduction	30
	3.2 Perturbation Solutions for Powers of α^{-1}	33
	3.3 Perturbation Solutions for Powers of α	38
	3.4 Asymptotic Method	50
4	GUIDANCE LAWS FOR THE ESCAPE AND CAPTURE PHASES	54
	4.1 Escape Phase	54
	4.2 Capture Phase	55
	4.3 A New Terminal Guidance Scheme	57
5	PLANET-SUN TRANSITION REGIONS	66
	NOTATION	70
	REFERENCES	72

SECTION 1

INTRODUCTION AND SUMMARY

This report deals with the problems of steering a vehicle from a circular orbit about one planet to a circular orbit about another planet using low thrust acceleration. The mission is usually divided into three phases: the planetary escape phase, the interplanetary transfer phase, and the planetary capture phase.

During the escape phase, the vehicle spirals many times around the planet until it reaches "escape," zero energy relative to the planet. It then departs along an asymptote, which direction is dictated by the position of the target planet. Very small thrust anomalies, on the order of one percent, are sufficient to cause a sizable error in the direction of the escape asymptote. The main guidance problem is to minimize this error.

During the interplanetary transfer phase the vehicle moves from the vicinity of the departure planet to the vicinity of the target planet. This is a two point boundary value problem to be satisfied by the appropriate thrust steering program.

The capture phase commences when the capture condition, zero energy relative to the target planet, is reached. For nominal conditions, the capture phase is simply the reverse of the escape phase; that is, the vehicle spirals toward the planet and approaches a circular orbit about the planet. The problem during the capture phase is to steer the vehicle to the desired circular orbit starting with off-nominal conditions at capture.

The interplanetary transfer phase is dealt with in Section 2. Previous studies are divided along two lines:

(1) Those using aids such as the energy-momentum diagram to patch rather simple steering programs to match the desired boundary conditions.

(2) Those using the indirect method of the calculus of variations and an extensive computer program to generate optimal steering programs.

The first approach was pursued by RODRIGQUEZ [1] , LEVIN [2] , FOX [3] , and MOECKEL [4] but has been dropped by more recent investigators because it does not directly provide optimal solutions.

Investigators using the second approach were led to consider steering programs which were progressively more simple and more realistic. This trend is noted below. IRVING and BLUM [5] in 1959 and MELBOURNE [6] in 1960 treated both the thrust magnitude and direction as the control variables. Next, MELBOURNE and SAUER [7] in 1962 and ZIMMERMAN, MACKAY, and ROSSA [8] in 1963 used segments of constant thrust linked by a coast segment. The thrust direction and the thrust durations were the control variables. In 1965, MELBOURNE and SAUER [9] determined optimal transfers for segments of constant thrust at fixed angles relative to the radial direction linked by a coast segment. The control variables were the two fixed steering angles and the thrust durations. MELBOURNE and SAUER demonstrate that this last steering program is only slightly less efficient than the more complicated steering programs.

While the trend is to more simple steering programs, the methods of analysis are no less complex. In Paragraph 2.5, it is shown that a complete picture of the transfer problem can be formed using the energy-momentum diagram to link segments of constant thrust acceleration at fixed steering angles with a coast segment. This endeavor goes well beyond the point reached in earlier studies [1-4] . Contours of constant characteristic velocity are presented as functions of the target planet lead angle and flight time for a matrix of steering angle combinations. The optimum steering combinations and the corresponding characteristic velocity requirements are presented as functions of flight time. The same results may be used to estimate the payload penalties for reduced flight times or for increasing the width of the launch window. Furthermore, simple analytic solutions to the powered segments, which enable one to make all the calculations with the aid of only a desk calculator, are presented.

The principal analytical methods for describing low thrust planetary escape and capture spirals are evaluated in Section 3. In this report α denotes the ratio of the thrust acceleration to the gravity acceleration in either the initial or final circular orbit. α is assumed to be a constant or zero

for any mission. For the escape and capture phases using ion propulsion, α typically ranges between 10^{-2} and 10^{-4}. ANTHONY [10] and others have generated a perturbation solution in powers of α^{-1} which accommodates a variety of steering programs. Their method is valid to the point of escape for $\alpha > 0.2$ and is of no particular use for smaller α. JOHNSON and STUMPF [11, 12] generated a second order perturbation solution in powers of α which they hoped would be valid to escape for very small α. It is demonstrated that this method is completely unsuited for small α, and in fact is valid to escape only for $\alpha > 0.2$. For $\alpha < 10^{-2}$ the solutions break down almost immediately. The asymptotic method employed by ZEE [13] and LASS and LORREL [14] was evaluated last. It was found to be valid over almost the entire trajectory, in fact up to the last revolution. During the last revolution, the eccentricity rapidly increases and the method breaks down. Attempts were made to combine the asymptotic and perturbation methods. These attempts were unsuccessful. In summary, the problem of obtaining an approximate analytic solution which is valid to the point of escape for $\alpha < 10^{-2}$ remains unsolved.

The escape and capture phases are treated numerically in Section 4. The escape problem, that of correcting the direction of the escape asymptote, is discussed in Paragraph 4.1. It is too costly in time and payload to correct the escape asymptote by thrust vector steering during the last revolution about the target planet. BATTIN and MILLER [15] would vary the thrust acceleration sometime shortly before the last revolution to make up for predicted errors in the asymptote. This method, while theoretically feasible, depends on the precise calculation of a very small corrective thrust. The method, recommended in this report, is to turn the thrust off for a short interval, sometime before the last revolution, when the orbit eccentricity is still small. The coast duration is analytically related to the asymptote orientation error.

The major portion of Section 4 deals with the problem of steering to a circular orbit starting from off-nominal conditions at capture. Unlike the escape problem, this problem cannot be disposed by simply varying the thrust level or by judiciously turning the thrust on and off. BATTIN and MILLER solve this problem by steering to a pseudo-reference path. Their method does not depend on an explicit solution to the trajectory.

An entirely different solution is developed in Paragraph 4.3; one which does not depend on an explicit solution or any reference path. The steering angle is controlled as a function of the instantaneous energy and velocity heading angle. Convergence is achieved even for large errors in the radial distance and the velocity heading angle at capture. Curves are presented which allow one to estimate the characteristic velocity as a function of the capture conditions using two different control gains.

While a feedback logic is developed for the capture phase, none is presented for the interplanetary phase. In fact the principal unsolved problem is

how to project errors from the interplanetary phase to errors at the start of the capture phase. Difficulties arise because the two phases are linked by a transition region in which the solar and planetary attractions are on the same order. This problem is discussed in Section 5.

SECTION 2

INTERPLANETARY TRANSFER

2.1 THE ENERGY MOMENTUM DIAGRAM

For the transfer phase of the mission, the assumption is made that the vehicle starts in a circular orbit about the Sun at one astronomical unit (1AU) and terminates in a circular orbit about the Sun at a radius equal to that of the target planet. The problem is to steer the vehicle between the two orbits using constant or zero thrust acceleration. The planetary attractions are ignored in the following discussion.

In general, solutions which satisfy the boundary conditions are found by trial and error. However, by mapping the transfer orbit on an energy-momentum (E-h) diagram, the problem can be split into two initial value problems, one commencing at the inner orbit and the other commencing at the outer orbit. In this way, the transfer orbit can be found directly without recourse to trial and error methods.

The idea of using the energy-momentum diagram was suggested by RODRIQUEZ [1] in 1959. His restrictions were somewhat different than ours. He had no coast segment but instead required two different acceleration levels to match end conditions. Our restrictions are more realistic. LEVIN [2] used the energy-momentum diagram to patch segments of constant circumferential and radial thrust acceleration linked by a coast phase. MOECKEL [4] attempted to use the E-h diagram to patch segments of constant tangential thrust acceleration, but was unable to link the two segments. This difficulty can be handled by a theorem on image trajectories. FOX [3] in 1959 successfully used an energy-eccentricity diagram to link segments of constant tangential thrust acceleration. His solutions provide the minimum characteristic velocity transfers for fixed thrust acceleration when there is no restriction on the total time of flight.

A hypothetical transfer trajectory and the corresponding E-h diagram are shown in Figure 2-1. The departure and target orbits are designated as points 1 and 2, respectively. The vehicle is powered from 1 to a, it coasts on a KEPLER ellipse from a to b, and is powered from b to 2. Since a and b lie on the same ellipse, they are coincident on the E-h diagram.

The procedure for obtaining the transfer orbit for specified thrust directions and thrust acceleration is as follows: The equations of motion for powered flight are integrated (either by approximate analytical techniques or numerical methods) from 1 to some point beyond the expected location of a. The corresponding trace on the E-h diagram is made. Next, the equations are integrated backwards from point 2 past the expected location of b. The corresponding trace is made on the E-h diagram. The intersection of the lines, corresponding to the two powered segments, on the E-h diagram locate points a and b on the transfer trajectory. A KEPLER ellipse is fitted between a and b. The parameters of greatest interest are the total flight time, the total powered time, and the polar angle θ between 1 and 2.

2.2 THE POWERED THRUST SEGMENTS

The geometry for the powered thrust segments is shown in Figure 2-2. The vehicle position P is defined in terms of the polar coordinates r and θ. The vehicle velocity $\bar{v}$ is expressed in terms of its magnitude v and direction ϕ with respect to the outward radial direction. The direction of the thrust acceleration f is specified either by the angle ψ relative to the outward radial direction or the angle β relative to $\bar{v}$. There are four special cases:

$\psi = 0$ radial thrust

$\psi = \pi/2$ circumferential thrust

$\beta = 0$ tangential thrust

$\beta = \pi/2$ normal thrust

It should be noted that ψ is time variable when β is fixed and vice versa.

When ψ is the control parameter, the equations of motion are conveniently espressed as

$$\dot{p}_r - \frac{h^2}{r^3} + \frac{km}{r^2} = f \cos \psi \qquad (2\text{-}1)$$

$$\dot{r} = p_r \qquad (2\text{-}2)$$

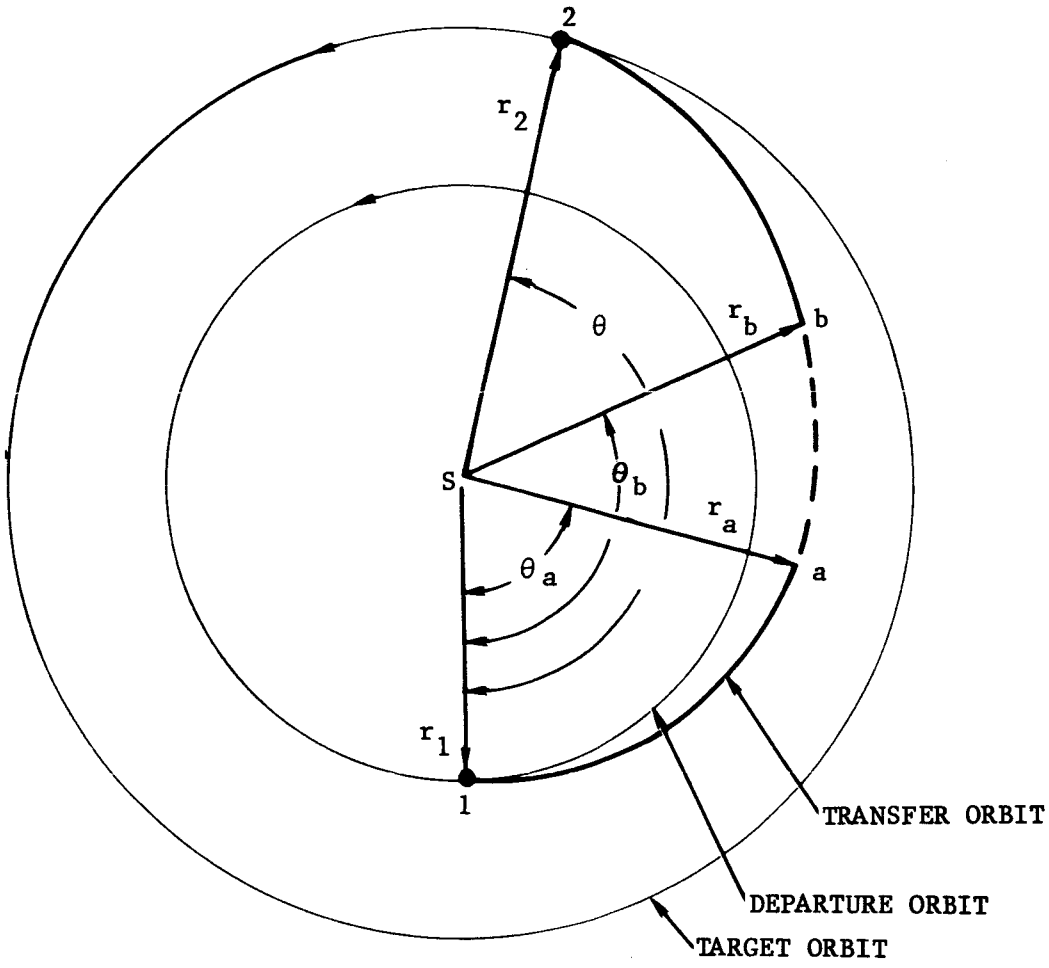

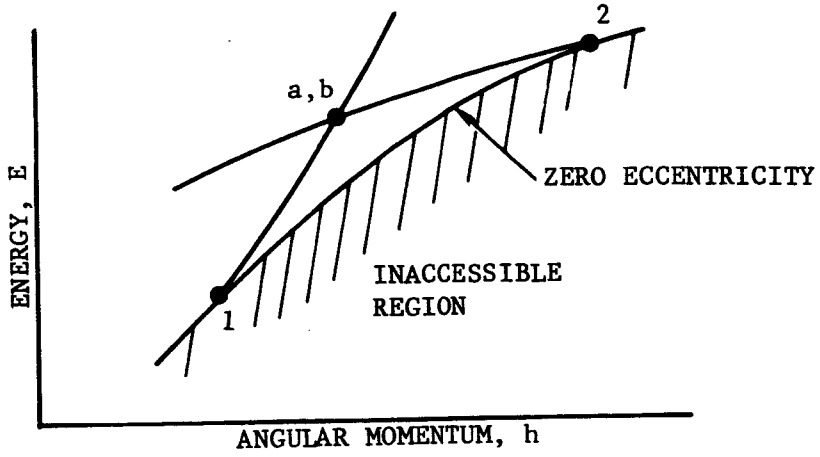

FIGURE 2-1. TRANSFER ORBIT GEOMETRY AND E-h DIAGRAM

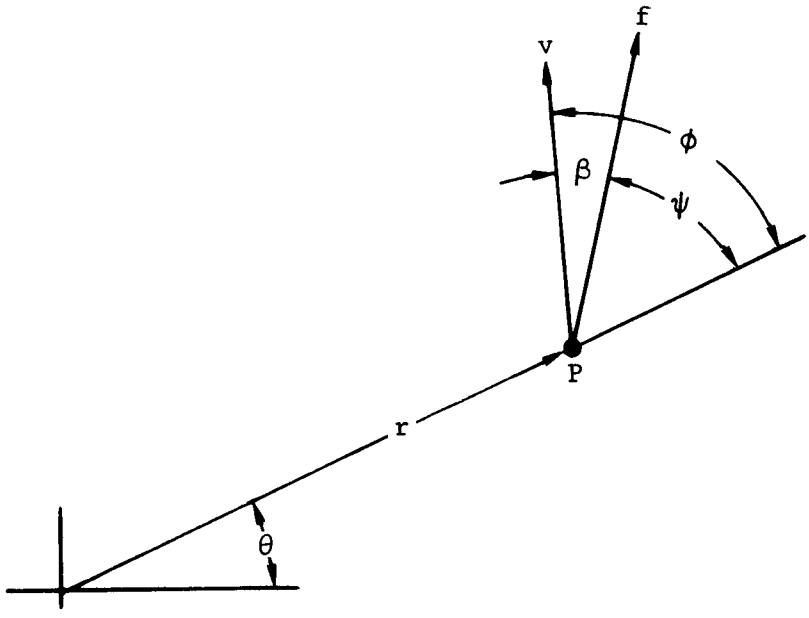

FIGURE 2-2. VELOCITY AND THRUST VECTOR GEOMETRY

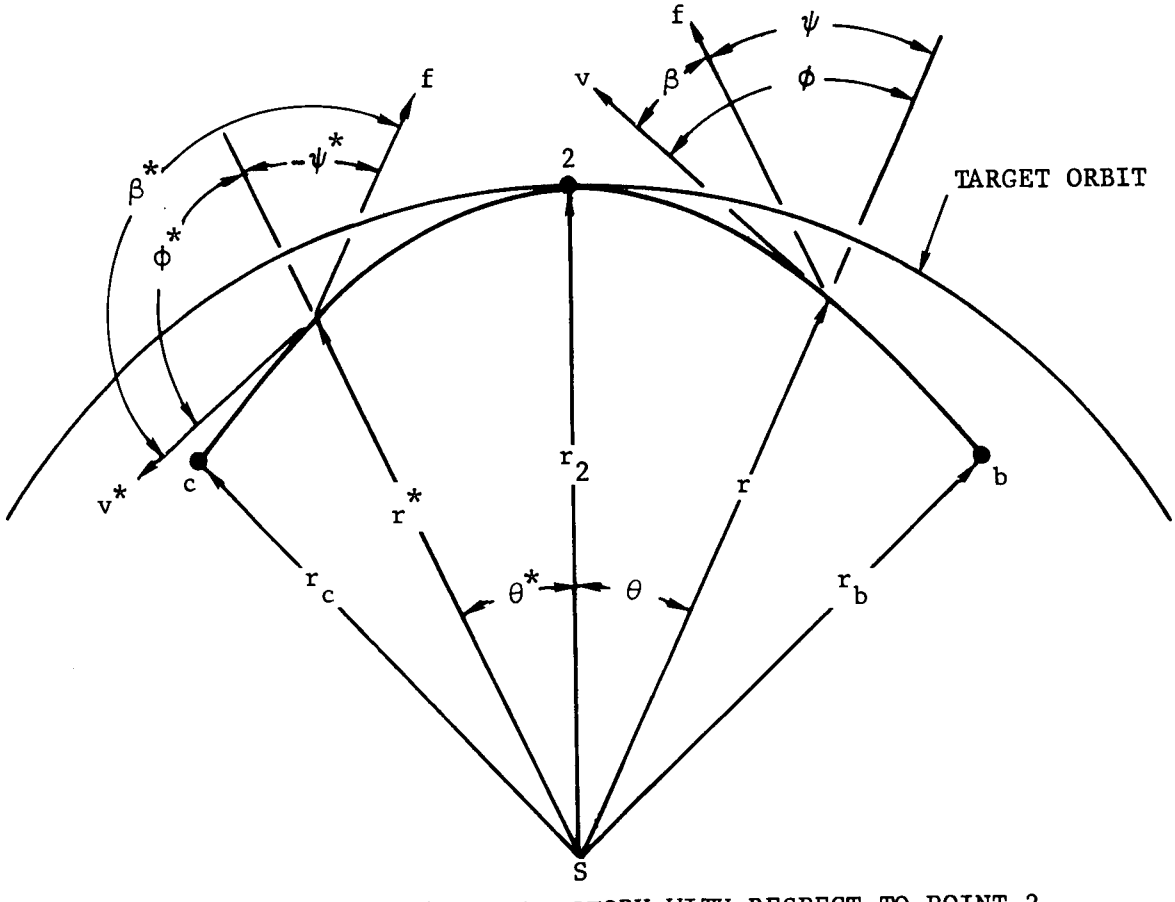

FIGURE 2-3. IMAGE TRAJECTORY WITH RESPECT TO POINT 2

$$\dot{h} = fr \sin\psi \tag{2-3}$$

$$\dot{\theta} = h/r^2 \tag{2-4}$$

where k is the universal constant of gravitation, m is the mass of the attracting body (the Sun in this case), and h is the angular momentum about the attracting body.

On the other hand, when β is the control parameter, the equations are more conveniently expressed as

$$\dot{v} = -\frac{km}{r^2}\cos\phi + f\cos\beta \tag{2-5}$$

$$\dot{\phi} = \left(\frac{km}{r^2} - \frac{v^2}{r}\right)\frac{\sin\phi}{r} - \frac{f\sin\beta}{v} \tag{2-6}$$

$$\dot{r} = v\cos\phi \tag{2-7}$$

$$\dot{\theta} = \frac{v}{r}\sin\phi \tag{2-8}$$

As described earlier, the vehicle is powered from b to 2. However, in determining the transfer orbit, b is unknown. Consequently, one must start with circular orbit conditions at 2 and integrate backwards to find b. In practice, one calculates the image trajectory 2 to c (where c is the image point of b), and by reflection obtains the desired trajectory b to 2. This may be seen by carrying out a coordinate transformation of the equation sets (2-1, 2, 3, 4) and (2-5, 6, 7, 8) by the method described by MIELE [16].

Equations (2-1) through (2-4) remain invariant under the transformation

$$p_r^* = -p_r, \quad r^* = r, \quad h^* = h, \quad \theta^* = -\theta, \quad \tau^* = -\tau, \quad \psi^* = -\psi$$

Similarly, Equations (2-5) through (2-8) remain invariant under the transformation

$$v^* = v, \quad \phi^* = \pi - \phi, \quad r^* = r, \quad \theta^* = -\theta, \quad \tau^* = -\tau, \quad \beta^* = \pi - \beta$$

The starred variables (except for τ^*) are pictured in Figure 2-3. The invariance of the equations of motion suggests that the solution going from 2 to c may be used to obtain the image trajectory from 2 to b. This ruse was used to obtain the transfer orbits in this section.

It should be noted that the theorem on image trajectories does not apply when the thrust acceleration is a variable. Without this aid the two point boundary value problem cannot be reduced to two initial value problems.

2.3 SOLUTIONS USING TANGENTIAL THRUST ACCELERATION

EDELBAUM [17] has shown that the absolute minimum characteristic velocity for a transfer between coplanar circular orbits with radii ratios less than 12 is defined by an impulsive HOHMANN transfer. Low thrust transfers require greater characteristic velocities than impulsive transfers, but the differences are small when the orbit radii ratios are less than 2.

For a HOHMANN transfer, the thrust is applied tangentially. Therefore, it is logical to first consider tangential thrust steering programs for low thrust transfers. The results which follow largely duplicate those obtained by FOX [3], whose work had been overlooked.

The transfer orbits were generated using the E-h diagram with powered thrust segments obtained by numerical integration of the set (2-5) through (2-8) with $\beta = 0$. The results are expressed in units normalized on the inner orbit parameters. Specifically, the radial distance, time, and the thrust acceleration are expressed in the nondimensional units

$$\rho = \frac{r}{r_1}, \qquad \tau = \sqrt{\frac{km_1}{r_1^3}}\, t, \qquad \alpha = \frac{fr_1^2}{km_1}$$

Transfer orbits were calculated for combinations of thrust acceleration $\alpha = 0.5$, 0.2, 0.1, 0.05, and 0.02 and final orbit radii $\rho_2 = 1.2$, 1.228, 1.5, 2, 5, and 10. The important transfer orbit characteristics are listed in Table 2-1. The energy and momentum of the intermediate KEPLER orbit are designated by E_{ab} and h_{ab}, respectively. The radial distances at a and b are tabulated in the next two columns. These four parameters define the segment of the transfer ellipse. The polar angles θ_a, θ_b, and θ_2 define the range angles at a, b, and 2 measured from 1. Likewise τ_a, τ_b and τ_2 give the normalized time in radians of travel at the inner orbit starting at 1. τ_p denotes the total powered time interval and $\alpha\tau_p$ denotes the characteristic velocity.

The characteristic velocity $\alpha\tau_p$ is plotted in Figure 2-4 as a function of ρ_2 for selected thrust acceleration levels α. Also shown is the characteristic velocity for the HOHMANN transfer given by the equation

$$\alpha\tau_p = \sqrt{\frac{2\rho_2}{1+\rho_2}} - 1 + \frac{1}{\sqrt{\rho_2}}\left(1 - \sqrt{\frac{2}{1+\rho_2}}\right) \qquad (2\text{-}9)$$

The difference between the low thrust transfer and the impulse transfer is negligible for $\rho < 2$. On this basis, it is concluded that the combination of two tangential thrust segments linked by a coast segment is optimal

TABLE 2-1

DATA FOR TRANSFERS BETWEEN COPLANAR CIRCULAR ORBITS

α	ρ_2	E_{12}	h_{12}	ρ_a	ρ_b	θ_a (deg)	θ_b (deg)	θ_2 (deg)	τ_a	τ_b	τ_2	τ_p	$\alpha\tau_p$
0.5	1.228	0.903	1.047	1.0002	1.2279	5.5	8.7	188.7	0.094	3.470	3.541	0.170	0.085
	1.5	0.802	1.094	1.0011	1.4995	11.3	16.5	183.9	0.189	4.361	4.595	0.364	0.182
	2.0	0.666	1.155	1.0053	1.9991	19.1	23.9	187.1	0.314	5.615	5.868	0.566	0.283
	5.0	0.332	1.292	1.0367	4.9994	37.6	39.1	184.9	0.584	15.34	15.72	0.974	0.487
	10	0.1815	1.355	1.0627	9.9998	45.5	45.97	198.3	0.698	39.52	39.92	1.062	0.531
0.2	1.2	0.915	1.041	1.0006	1.1994	12.0	21.8	176.5	0.208	3.382	4.738	0.425	0.085
	1.5	0.803	1.094	1.0072	1.4971	28.2	41.2	203.8	0.471	4.562	5.000	0.910	0.182
	2.0	0.666	1.157	1.0325	1.9955	47.4	59.3	211.7	0.779	6.050	6.693	1.425	0.285
	5.0	0.330	1.316	1.2153	4.9964	89.8	93.5	220.5	1.513	16.13	17.02	4.930	0.986
	10	0.18051	1.395	1.3619	9.9990	105.3	106.42	222.8	1.849	41.00	41.85	27.30	0.546
0.1	1.2	0.907	1.046	1.0032	1.1982	26.7	44.3	218.0	0.471	3.960	4.350	0.880	0.088
	1.5	0.797	1.099	1.0306	1.4898	57.8	82.6	223.6	0.973	4.525	5.355	1.84	0.184
	2.0	0.661	1.165	1.1236	1.9790	93.4	116.6	235.4	1.610	5.935	7.188	2.86	0.286
	5.0	0.3231	1.3845	1.6967	4.9863	161.0	168.1	266.4	3.315	17.41	19.13	5.01	0.501
	10	0.18115	1.5105	2.0654	9.9963	197.6	199.80	297.7	4.100	42.60	44.23	5.76	0.576
0.05	1.228	0.897	1.051	1.0175	1.2241	59.0	88.5	204.6	1.012	4.260	4.342	1.70	0.085
	1.5	0.795	1.102	1.1078	1.4633	113.2	162.2	259.6	1.992	4.572	6.202	3.62	0.181
	2.0	0.6399	1.205	1.4260	1.9468	184.2	224.5		3.665			5.78	0.289
	5.0	0.29357	1.6258	2.5731	4.9816	282.6	293.4	397.3	9.210	22.18	24.68	10.82	0.541
	10	0.16759	1.8576	3.1536	9.9928	305.2	308.94	407.2	10.02	51.30	53.90	12.62	0.632
0.02	1.2	0.906	1.048	1.0646	1.1630	132.5	157.3	454.6	2.340	3.978	5.980	4.35	0.087
	1.5	0.692	1.200	1.4207	1.4982	375.7	463.2	617.3	8.210	9.900	10.70	9.00	0.180
	2.0	0.5715	1.310	1.6630	1.9606	488.5	540.0	790.2	12.03	15.42	17.06	14.70	0.294
	5.0	0.2653	1.838	3.2219	4.9650	680.0	698.7	830.6	23.40	38.52	42.55	27.40	0.548
	10	0.15401	2.1634	4.1916	9.9777	720.2	727.85		28.10	72.75	77.70	33.15	0.663

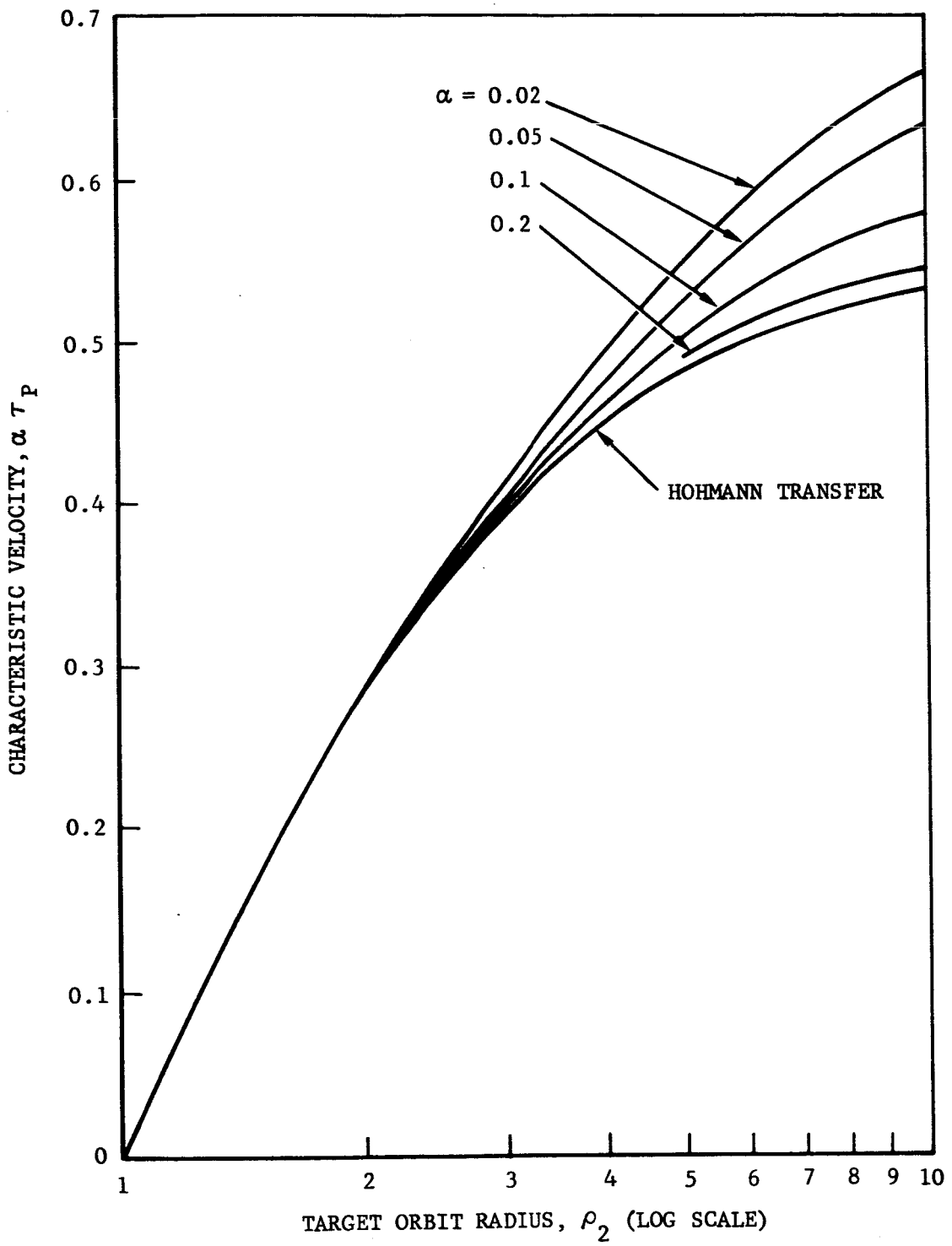

FIGURE 2-4. CHARACTERISTIC VELOCITY

if no restriction is placed on total flight time. This observation was not made by FOX. The flight times for the powered thrust segments and the total flight time are plotted as function of α in Figure 2-5. In all cases, the total flight time increases as the thrust acceleration decreases. Likewise, the total range angle θ_b shown in Figure 2-6 increases as the α decreases.

2.4 REVIEW OF OPTIMAL SOLUTIONS FOR RESTRICTED FLIGHT TIMES

ZIMMERMAN, MACKAY, and ROSSA [8] presented results of an extensive computer study for optimal transfer from Earth to Mars using segments of constant thrust linked by a coast segment. The steering angle and thrust durations were the control variables for obtaining minimum characteristic velocity transfers for specified initial thrust to weight ratios. They obtained results with and without constraints on flight time.

With no constraint on flight time, they show that ψ should be close to $\pi/2$ (or what is almost equivalent, that β should be close to 0) for both thrust segments. The results plotted in Figure 2-4 are in close agreement with this conclusion.

For flight times, shorter than obtained using tangential thrust, ZIMMERMAN, MACKAY and ROSSA show that ψ should be tilted toward the outward radial direction during the first thrust segment, and inward during the second thrust segment to maximize the payload. The powered segments are longer in duration, but the coast segment is shorter. As a result, the characteristic velocity requirement increases as the flight time decreases. This same result was obtained independently by MELBOURNE and SAUER [7].

There is a lower limit on flight time for a given thrust level, occurring when the coast phase vanishes. This limiting case was solved by FAULDERS [18] in 1961. FAULDERS' optimal thrust steering program for $\rho_2 = 1.5$ and $\alpha = 0.1667$ is shown in Figure 2-7. For this example, the normalized flight time τ is 3.22 and the characteristic velocity $\alpha\tau_p$ is 0.537. This compares with $\tau = 5.50$ and $\alpha\tau_p = 0.177$ when no restriction is placed on the flight time.

The E-h path for FAULDERS' solution is shown in Figure 2-8. It exhibits a closed loop which intersects at E = -0.382 and h = 1.105. When the powered segment around the loop is replaced by a KEPLER ellipse with values of E and h defined by the intersection point on the loop, one finds a slightly larger τ (3.43 compared to 3.22), and a significantly smaller $\alpha\tau_p$ (0.312 compared to 0.537). This is indicative of the large propulsion penalty one pays for even small reductions in the flight time.

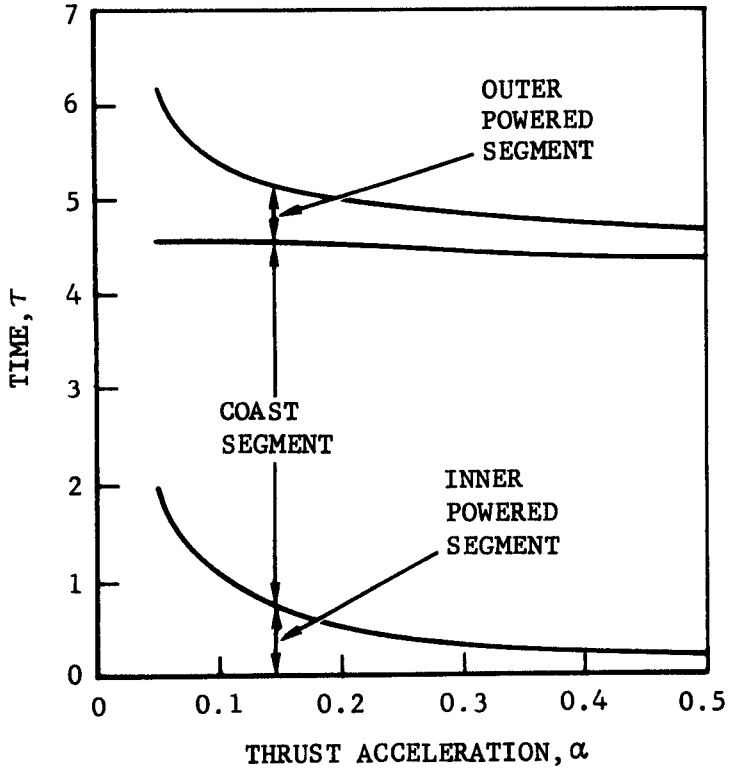

FIGURE 2-5a. FLIGHT TIME FOR $\rho_2 = 1.5$

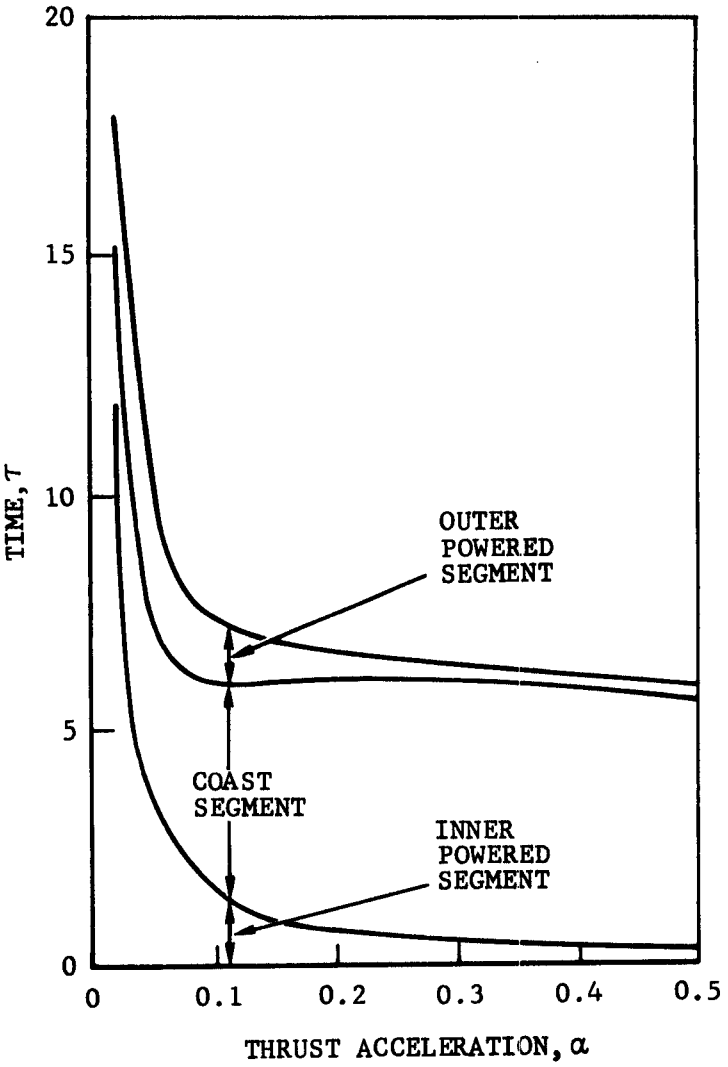

FIGURE 2-5b. FLIGHT TIME FOR $\rho_2 = 2.0$

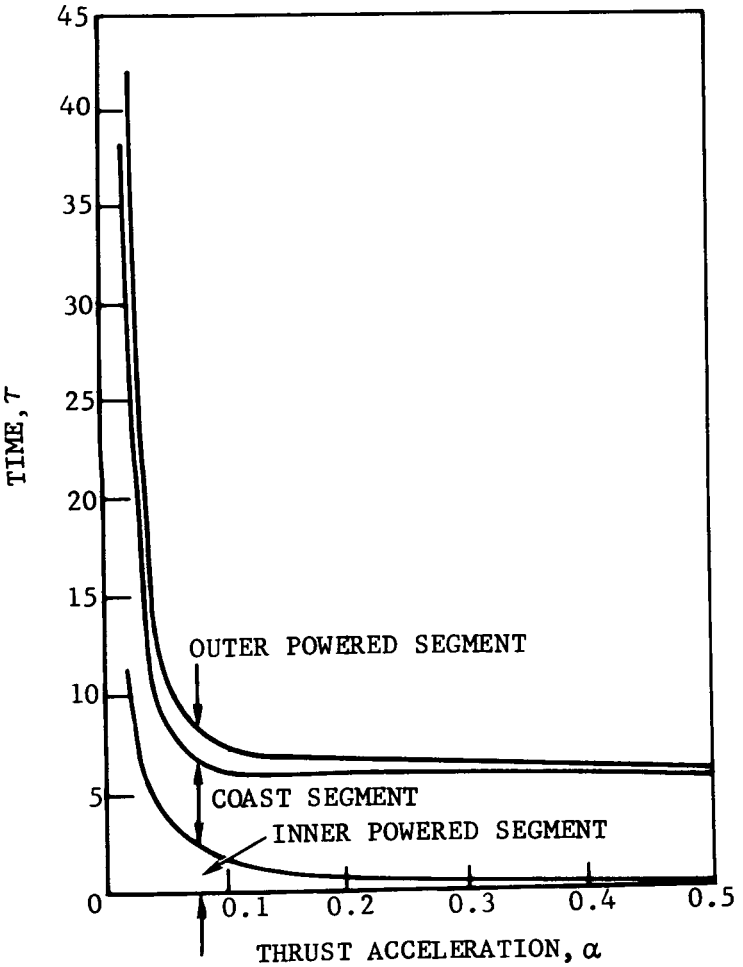

FIGURE 2-5c. FLIGHT TIME FOR $\rho_2 = 5$

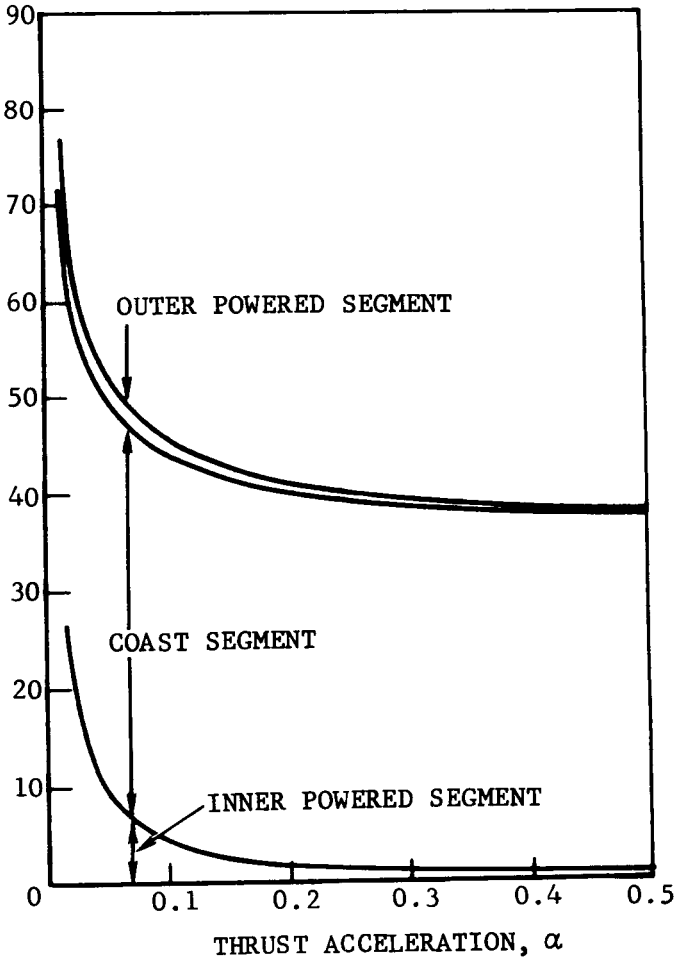

FIGURE 2-5d. FLIGHT TIME FOR $\rho_2 = 10$

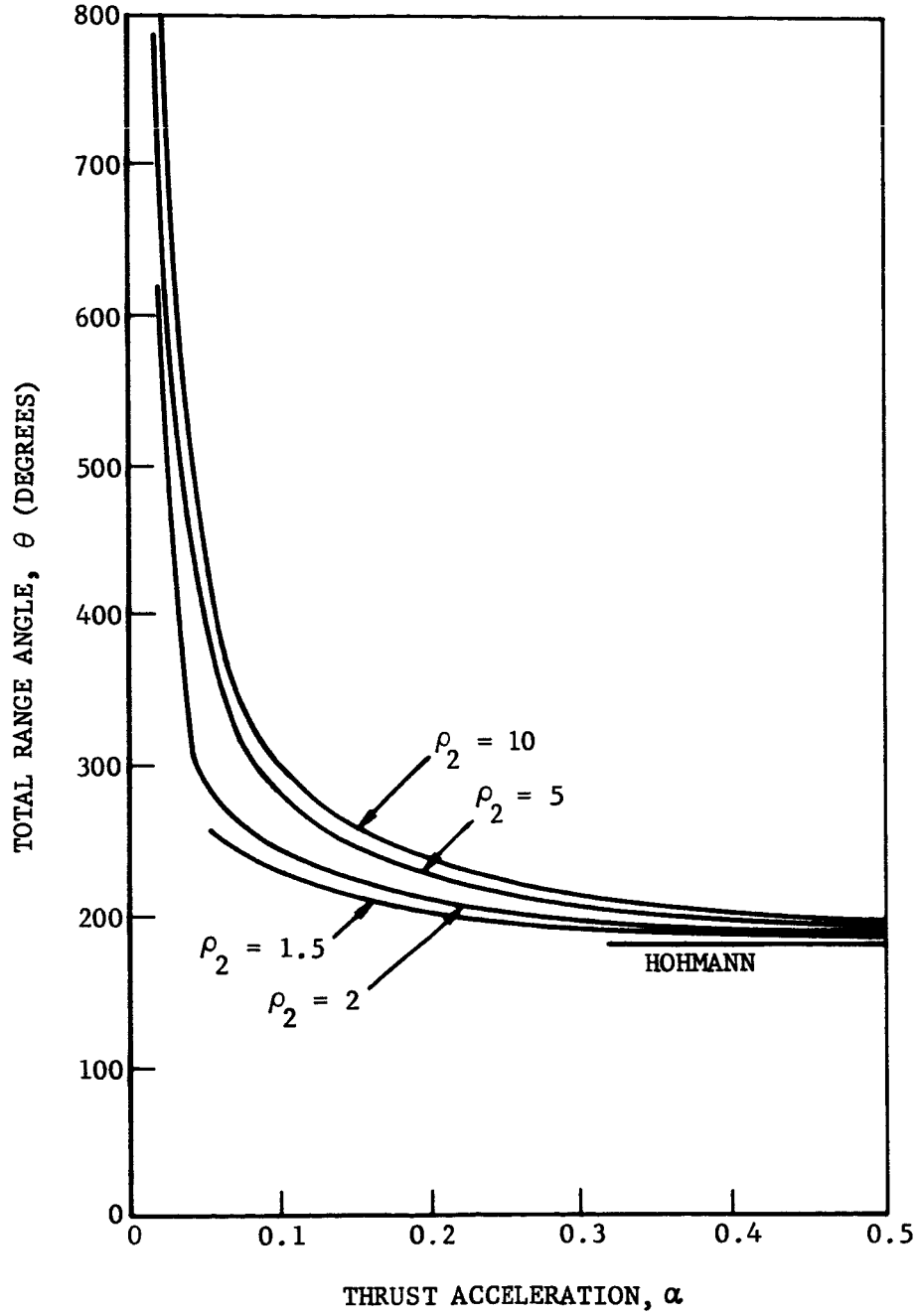

FIGURE 2-6. RANGE ANGLE

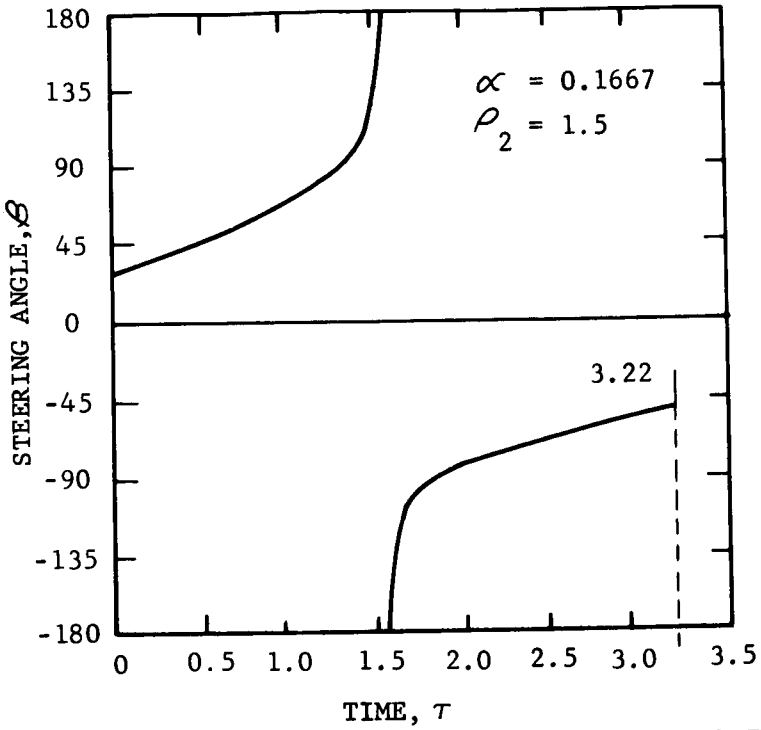

FIGURE 2-7. OPTIMUM STEERING ANGLE FOR CONTINUOUS THRUST [18]

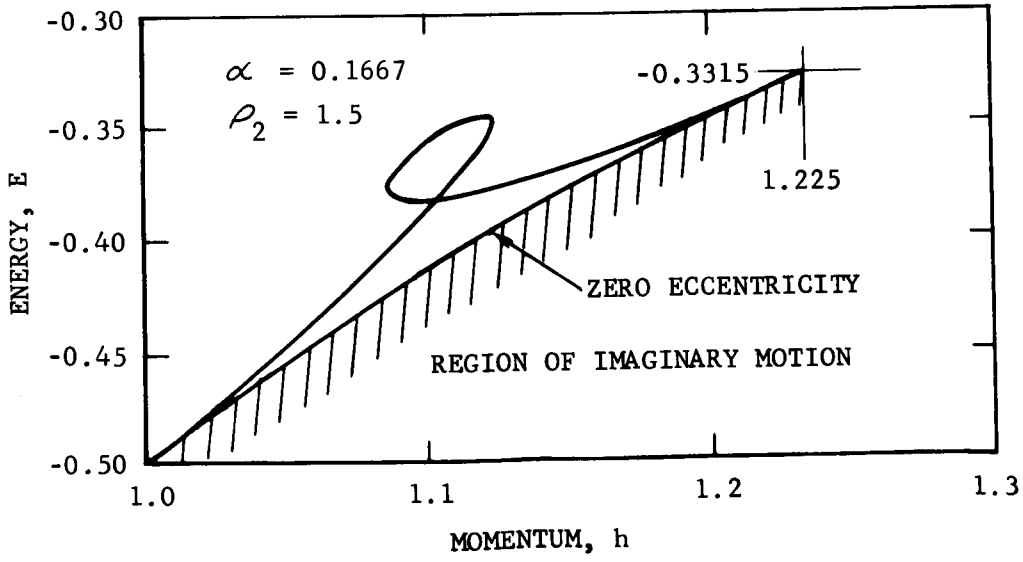

FIGURE 2-8. E-h DIAGRAM FOR OPTIMUM STEERING PROGRAM

MELBOURNE and SAUER [9] studied the transfer problem when ψ_1 (the steering angle during the first thrust segment) and ψ_2 (the steering angle during the second thrust segment) are held constant. They determined the values of ψ_1 and ψ_2 which maximize the payload for specified flight time. Comparing these results with those obtained earlier [7] for variable ψ, MELBOURNE and SAUER found only small differences in payload capability. The obvious conclusion is that simple steering programs using fixed ψ_1 and ψ_2 can provide near optimum results.

2.5 ANALYTIC SOLUTIONS FOR CONSTANT STEERING ANGLES

Approximate analytic solutions for the powered thrust segments of the transit phase with ψ held constant can be obtained by the method described below. The model geometry is shown in Figure 2-9 where S denotes the Sun, P_i denotes the planet (i = 1 for Earth and 2 for Mars) and P denotes the vehicle. P_i moves in a circular orbit with radius r_i and angular rate n about S. The position of P may be defined in terms of either the inertial XY coordinates with origin at S or the rotating xy coordinates with origin at P_i. The method of solution is based on the observation that for typical, near optimum Earth to Mars or Earth to Venus transfers, x and y remain small compared to r_i.

The transformation between XY and xy coordinates is given by

$$\left.\begin{aligned} X &= (r_i + x)\cos nt - y \sin nt \\ Y &= (r_i + x)\sin nt + y \cos nt \end{aligned}\right\} \qquad (2\text{-}10)$$

The time derivatives of X and Y are

$$\left.\begin{aligned} \dot{X} &= \dot{x}\cos nt - \dot{y}\sin nt - n(r_i + x)\sin nt - ny\cos nt \\ \dot{Y} &= \dot{x}\sin nt + \dot{y}\cos nt + n(r_i + x)\cos nt - ny\sin nt \end{aligned}\right\} \qquad (2\text{-}11)$$

and the kinetic energy per unit mass is

$$\begin{aligned} T &= \frac{1}{2}(\dot{X}^2 + \dot{Y}^2) \\ &= \frac{1}{2}\left[\dot{x}^2 + \dot{y}^2 + 2n(x\dot{y} - y\dot{x}) + n^2(x^2 + y^2) + 2n\, r_i\, \dot{y} + n^2 r_i(r_i + 2x)\right] \end{aligned} \qquad (2\text{-}12)$$

Planetary attractions are ignored in the transit phase. The gravitational attraction of the Sun is derivable from the potential function

$$V = -km/r \qquad (2\text{-}13)$$

where k is the universal constant of gravitation and m is the mass of the Sun. For x and y small compared to r_i, V can be approximated by,

$$V = -km\left[\frac{1}{r_i} - \frac{x}{r_i^2} + \frac{1}{r_i^3}\left(x^2 - \frac{y^2}{2}\right)\right] \qquad (2\text{-}14)$$

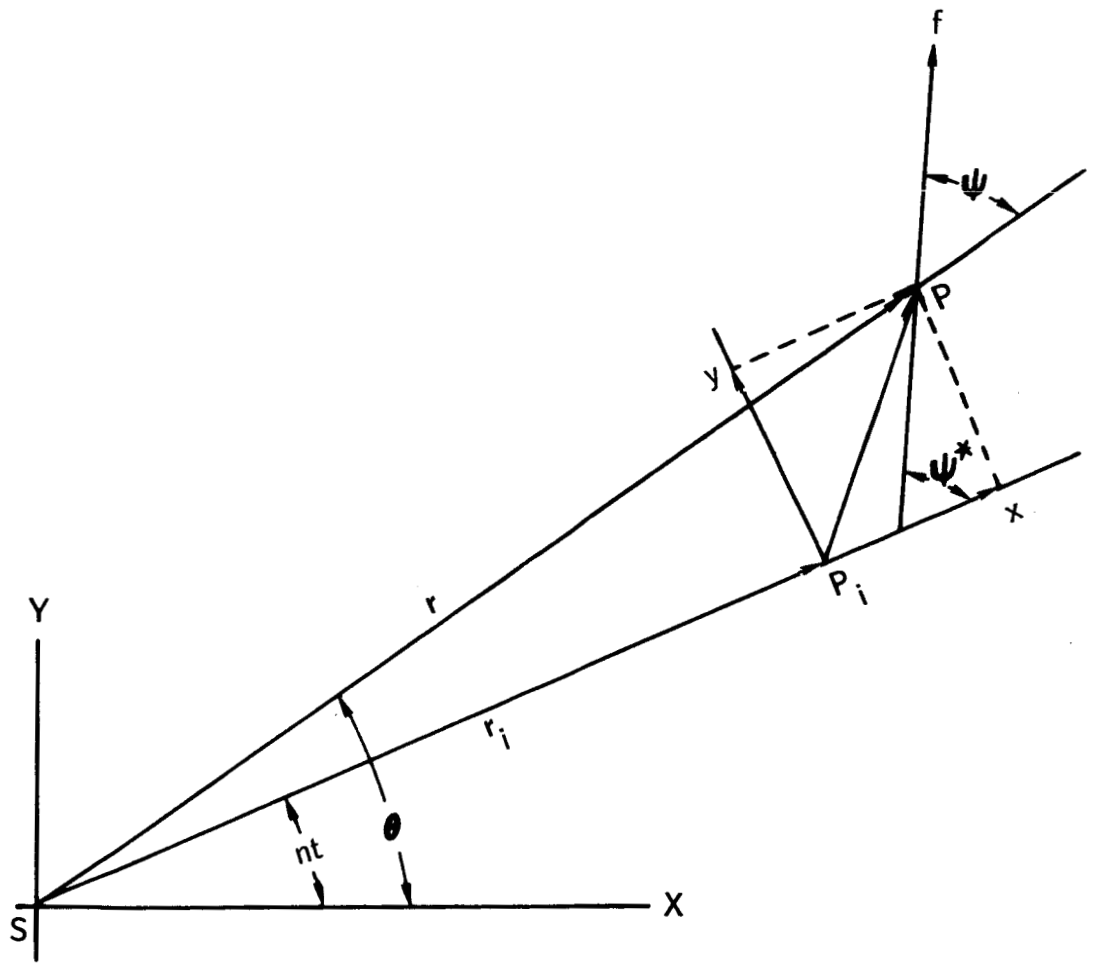

FIGURE 2-9. GEOMETRY USING A ROTATING COORDINATE SYSTEM

Using the relation $n^2 = km/r_i^3$, V becomes

$$V = -n^2\left(r_i^2 - r_i\, x + x^2 - \frac{y^2}{2}\right) \tag{2-15}$$

The total energy E = T + V and the angular momentum $h = X\dot{Y} - Y\dot{X}$ are given by

$$E = \frac{1}{2}\left[\dot{x}^2 + \dot{y}^2 + 2n(x\dot{y} - y\dot{x}) + n^2(2y^2 - x^2) + 2n\, r_i\, \dot{y} + n^2\, r_i\, (4x - r_i)\right] \tag{2-16}$$

$$h = r_i\left[\dot{y} + n\,(r_i + 2x)\right] \tag{2-17}$$

The equations of motion are obtained using the Lagrangian formulation

$$\left.\begin{aligned} \frac{d}{dt}\frac{\partial L}{\partial \dot{x}} - \frac{\partial L}{\partial x} &= f\cos\psi^* \\ \frac{d}{dt}\frac{\partial L}{\partial \dot{y}} - \frac{\partial L}{\partial y} &= f\sin\psi^* \end{aligned}\right\} \tag{2-18}$$

where L = T - V, f is the thrust acceleration and ψ^* is the angle between f and the x axis. For x and y small compared to r_i (the basic assumption in the analysis) the angle ψ^* is approximately equal to ψ. The explicit forms of the equations of motion are

$$\left.\begin{aligned} \ddot{x} - 2n\dot{y} - 3n^2x &= f\cos\psi^* \\ \ddot{y} + 2n\dot{x} &= f\sin\psi^* \end{aligned}\right\} \tag{2-19}$$

These equations are normalized by taking

$$\xi = x/r_i, \qquad \eta = y/r_i, \qquad \tau = nt, \qquad \alpha = f/(n^2 r_i)$$

In terms of the above parameters, the equations become

$$\begin{aligned} \xi'' - 2\eta' - 3\xi &= \alpha\cos\psi^* \\ \eta'' + 2\xi' &= \alpha\sin\psi^* \end{aligned} \tag{2-20}$$

where primes denote derivatives with respect to τ. In these units, E and h become

$$E = \frac{1}{2}\left[\xi'^2 + \eta'^2 + 2(\xi\eta' - \eta\xi') + 2\eta^2 - \xi^2 + 2\eta' + 4\xi - 1\right] \tag{2-21}$$

$$h = \eta' + 1 + 2\xi \tag{2-22}$$

The solutions to (2-20) are

$$\left.\begin{aligned} \xi &= \xi_o + 3\xi_o (1 - \cos\tau) + \xi_o' \sin\tau + 2\eta_o' (1 - \cos\tau) \\ &\quad + 2\alpha \sin\psi^* (\tau - \sin\tau) \\ \eta &= -6\xi_o (\tau - \sin\tau) + \eta_o - 2\xi_o' (1 - \cos\tau) - 3\eta_o' \tau + 4\eta_o' \sin\tau \\ &\quad + \alpha\left[4 \sin\psi^* (1 - \cos\tau) - \frac{3}{2}\sin\psi^* \tau^2 - \frac{1}{2}\cos\psi^* \tau\right] \end{aligned}\right\} \tag{2-23}$$

and their derivatives are

$$\left.\begin{aligned} \xi' &= 3\xi_o \sin\tau + \xi_o' \cos\tau + 3\eta_o' \sin\tau + 2\alpha \sin\psi^* (1 \cos\tau) \\ \eta' &= -6\xi_o (1 - \cos\tau) - 2\xi_o' \sin\tau - 3\eta_o' + 4\eta_o' \cos\tau \\ &\quad + \alpha\left(4 \sin\psi^* \sin\tau - 3 \sin\psi^* \tau - \frac{1}{2}\cos\psi^*\right) \end{aligned}\right\} \tag{2-24}$$

If the vehicle starts in a circular orbit at radius r_i, the initial values ξ_o, η_o, ξ_o', and η_o' are zero, and the solutions reduce to

$$\left.\begin{aligned} \xi &= 2\alpha \sin\psi^* (\tau - \sin\tau) \\ \eta &= \alpha\left[4 \sin\psi^* (1 - \cos\tau) - \frac{3}{2}\sin\psi^* \tau^2 - \frac{1}{2}\cos\psi^* \tau\right] \end{aligned}\right\} \tag{2-25}$$

$$\left.\begin{aligned} \xi' &= 2\alpha \sin\psi^* (1 - \cos\tau) \\ \eta' &= \alpha\left(4 \sin\psi^* \sin\tau - 3 \sin\psi^* \tau - \frac{1}{2}\cos\psi^*\right) \end{aligned}\right\} \tag{2-26}$$

Transfer trajectories between circular orbits with $r_1 = 1$ and $r_2 = 1.5$ were calculated for $\alpha = 0.2$ (normalized at r_1) and all combinations of the

steering angles ψ_1 = 75, 90, 105, 120, and 135 degrees, and ψ_2 = 45, 60, 75, 90, and 105 degrees. The two thrust segments and the coast segment for each combination were patched using the E-h diagram.

Characteristic velocity $\alpha\tau_p$ and the total range angle θ are plotted as functions of the total flight time in Figures 2-10 and 2-11, respectively. These figures were cross-plotted to obtain Figure 2-12, in which characteristic velocity contours and the steering angle combinations are shown as functions of the target planet lead angle θ_L and the total flight time. The lead angle is the central angle between the target planet P_2 and the vehicle P at the start of the transfer phase. θ_L is related to θ and τ at rendezvous by the equation

$$\theta_L = \theta - n_2 \tau \qquad (2\text{-}28)$$

where n_2 is the mean rate of P_2.

Figure 2-12 is most instructive. It shows that ψ_1 and ψ_2 should be approximately 90 degrees to minimize characteristic velocity, which agrees with the results in Paragraph 2.3. The lead angle for this case is 49.5 degrees. Figure 2-12 can be used to estimate the characteristic velocity penalty to be paid should θ_L differ from the nominal value due to either launch delays or time delays in reaching the planetary escape conditions. The characteristic velocity penalties may be determined with and without the flight time held fixed.

Figure 2-12 also shows the characteristic velocity penalty one pays to achieve shorter flight times. For any given τ, there is a unique combination of ψ_1 and ψ_2 which minimizes $\alpha\tau_p$. Figure 2-12 was used to generate the plots of optimum ψ_1 and ψ_2, and the corresponding $\alpha\tau_p$ shown in Figure 2-13. As τ decreases, ψ_1 decreases and ψ_2 increases. This agrees with the curves given by MELBOURNE and SAUER in Figure 4 of [9] for somewhat different values of r_2 and α.

MELBOURNE and SAUER and other investigators, who use the calculus of variations to determine optimal steering programs, must rely on extensive computer programs to solve the two-point boundary value problem. Not only must the equations be solved numerically, but they must be solved many times over to converge on a single solution. It is obviously expensive to generate a family of optimal solutions by this method as one or more parameters are varied.

The approach presented above is entirely different. No attempt is made to generate the optimal solutions directly. Rather the problem is "shotgunned" with a wide choice of steering combinations. Twenty-five combinations were used to generate the plots in Figure 2-12. Using the E-h diagram, each attempted solution satisfies the boundary conditions. The method is

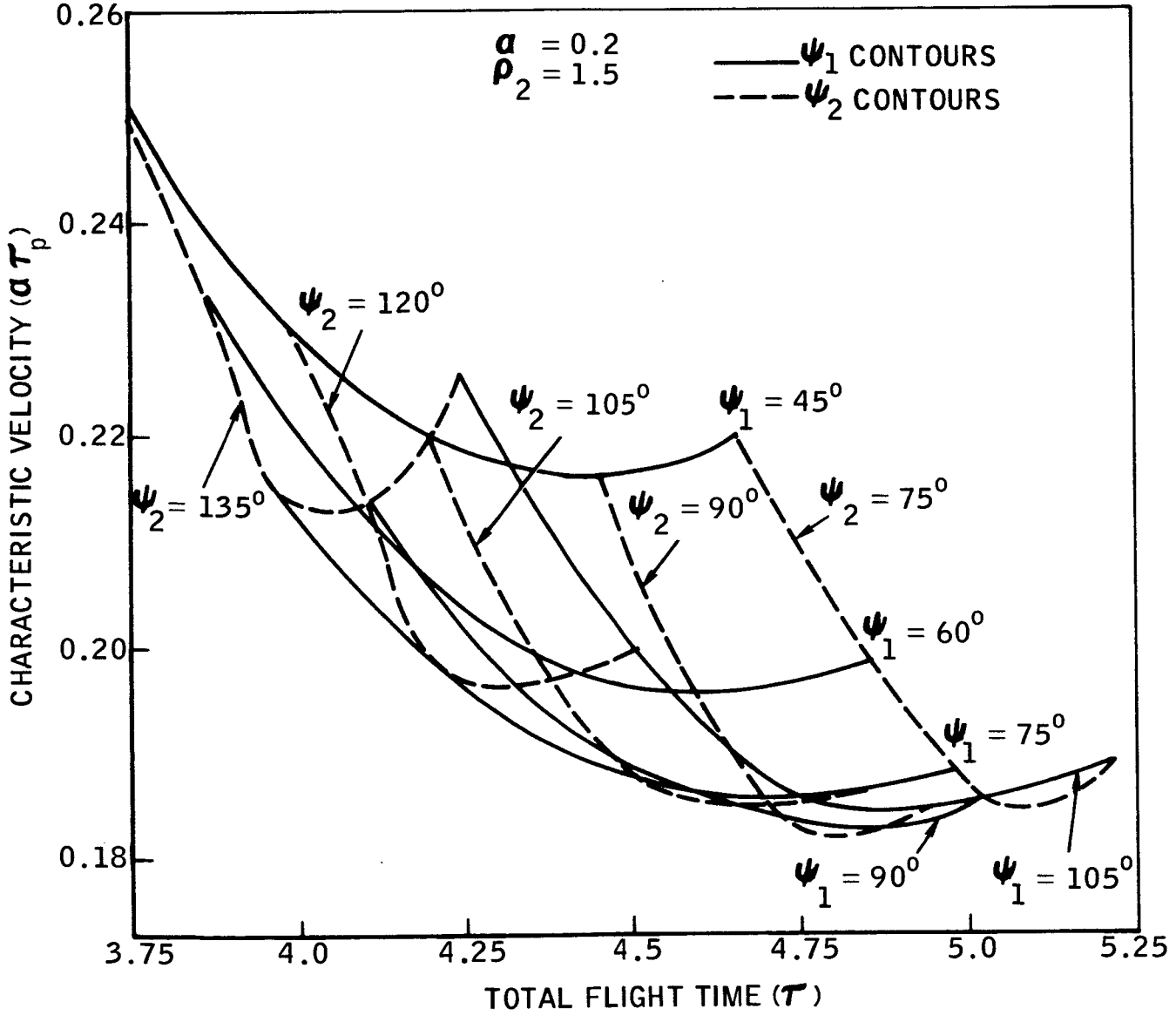

FIGURE 2-10. CHARACTERISTIC VELOCITY AS A FUNCTION OF THE TOTAL FLIGHT TIME FOR DIFFERENT STEERING ANGLE COMBINATIONS

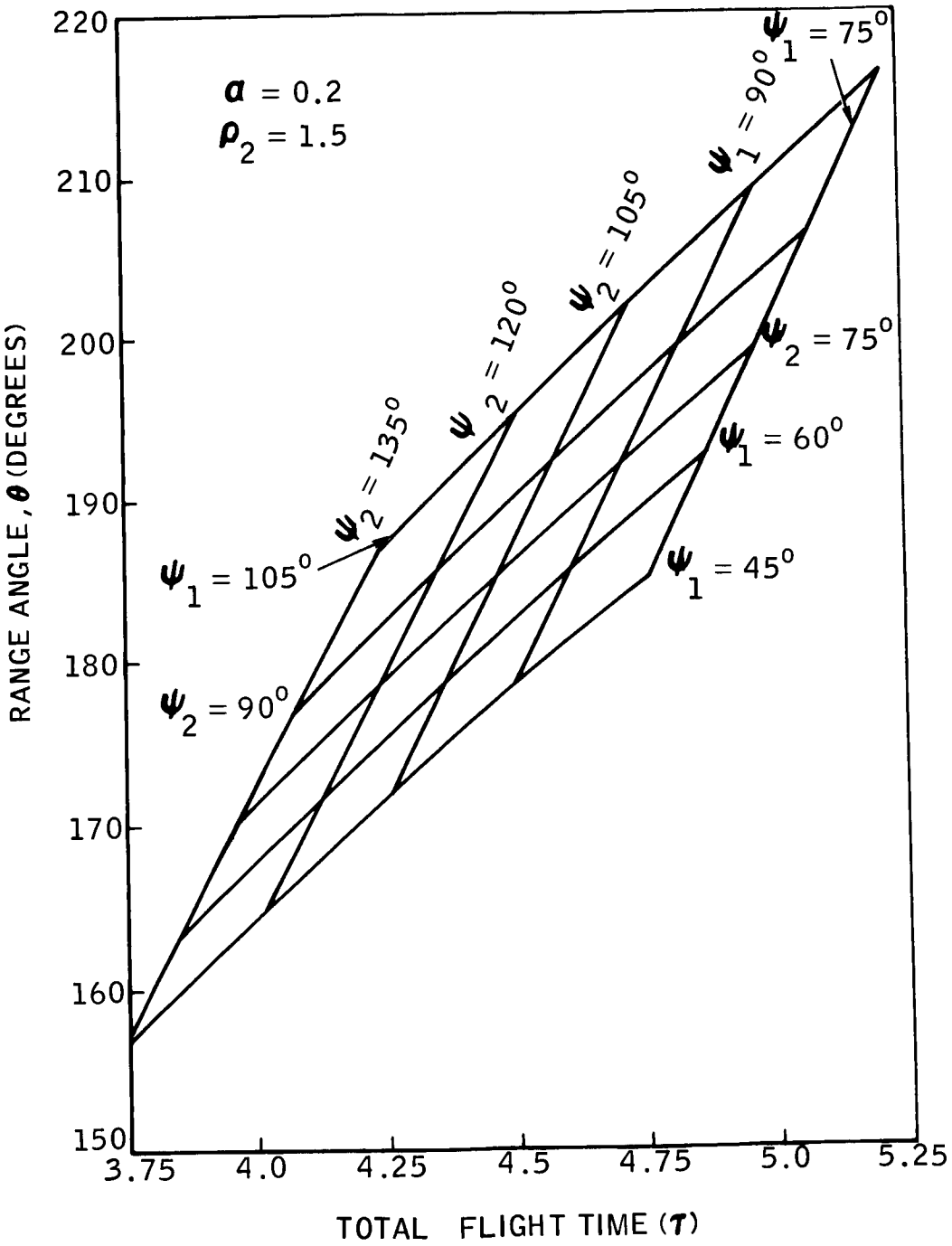

FIGURE 2-11. RANGE ANGLE AS A FUNCTION OF THE TOTAL FLIGHT TIME FOR DIFFERENT STEERING ANGLE COMBINATIONS

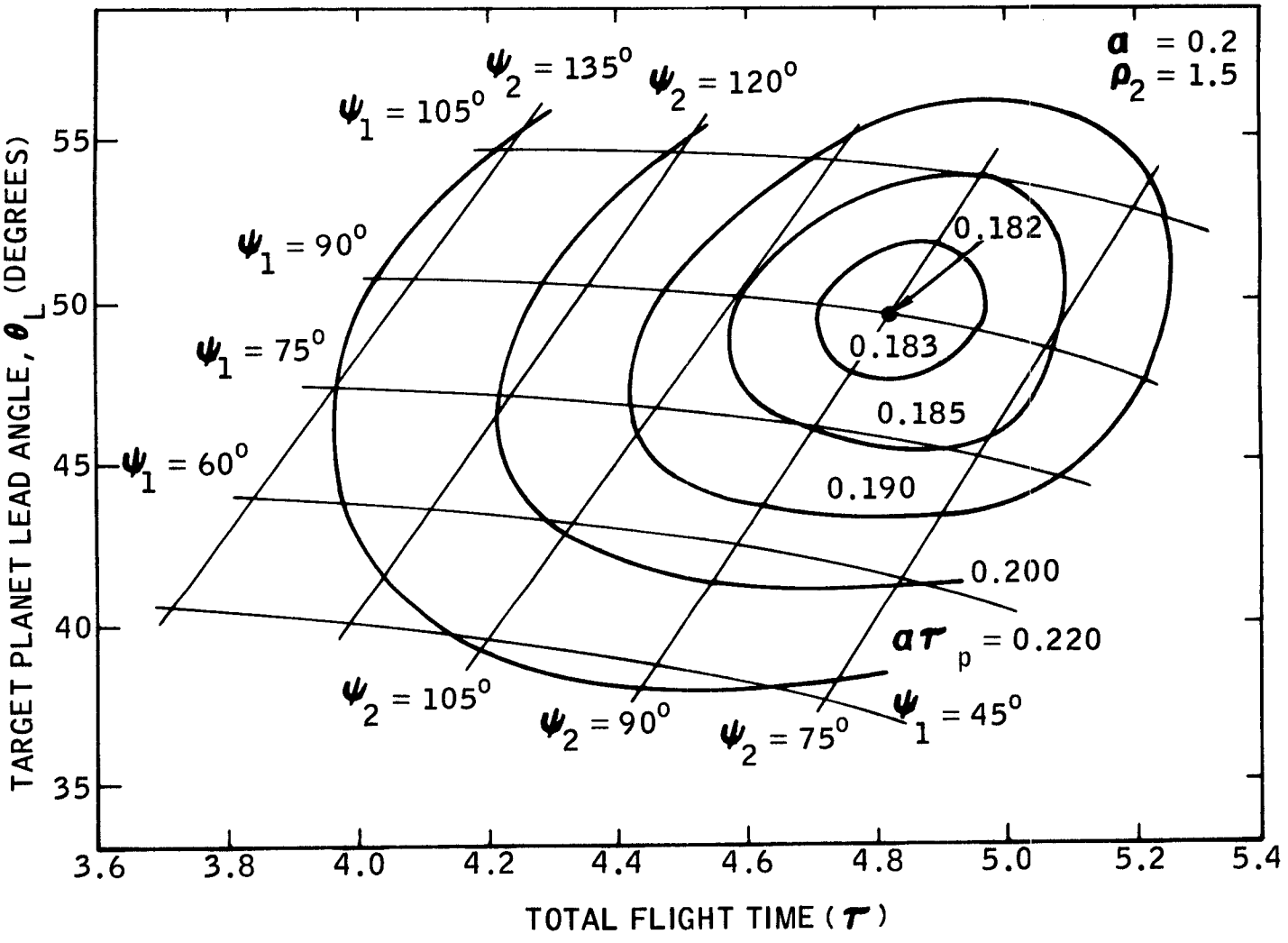

FIGURE 2-12. CHARACTERISTIC VELOCITY CONTOURS AND STEERING ANGLE COMBINATIONS

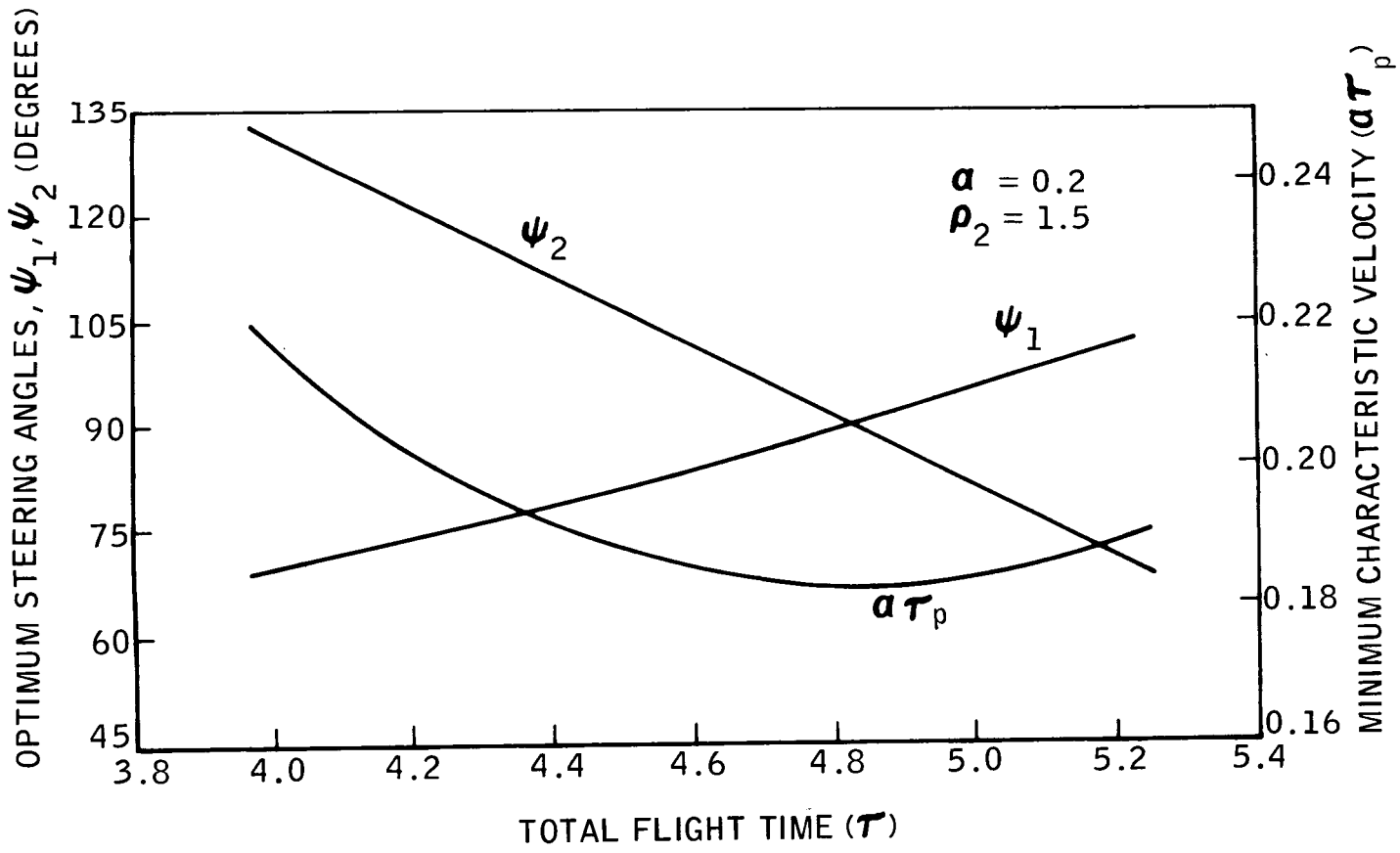

FIGURE 2-13. MINIMUM CHARACTERISTIC VELOCITY AND OPTIMUM STEERING ANGLES AS A FUNCTION OF THE TOTAL FLIGHT TIME

further facilitated by having analytical solutions for the individual thrust segments. When the results are plotted as in Figure 2-12, one obtains a mapping of the entire problem within the range of parameters considered. The $\alpha\tau_p$ contours allow one to determine the optimum steering combinations and the propulsion penalties one pays for flying nonoptimal courses. The fact that the nonoptimal solutions are presented thus appears as an advantage.

SECTION 3

APPROXIMATE ANALYTIC SOLUTIONS FOR PLANETARY ESCAPE AND CAPTURE

3.1 INTRODUCTION

The analytical methods for describing the escape and capture phases of a low thrust mission are compared and evaluated in this section. The methods of analysis may be divided into three groups:

(1) Perturbation solutions in powers of α^{-1} such as the works of TSIEN [19], BENNEY [20], LAWDEN [21], and ANTHONY [10].

(2) Perturbation solutions in powers of α such as the works of LEVIN [2], and JOHNSON and STUMPF [12].

(3) Asymptotoc solutions for small α such as the works of ZEE [13], and LASS and LORREL [14].

The main question is whether any of these methods can accurately describe the motion clear to escape using even the simplest of steering programs.

The numerical studies by PERKINS [22] provide a complete picture of low thrust escape from a circular orbit using constant tangential thrust acceleration. His solutions will serve as one basis for comparison of the analytical methods.

The geometry is shown in Figure 2-1. Let a zero subscript denote conditions in the initial circular orbit about the planet. In terms of the normalized parameters

$$\tau = \sqrt{\frac{km}{r_o^3}}\, t, \qquad \rho = \frac{r}{r_o}, \qquad k = \frac{h}{\sqrt{kmr_o}}$$

$$v = v\sqrt{\frac{r_o}{km}}, \qquad \mathcal{E} = \frac{r_o E}{km}, \qquad a = \frac{fr_o^2}{km}$$

where m is the mass of the attracting planet, the set (2-1) to (2-4) becomes

$$\rho'' - \frac{k^2}{\rho^3} + \frac{1}{\rho^2} = a\cos\psi \tag{3-1}$$

$$k' = a\rho\sin\psi \tag{3-2}$$

$$\theta' = \frac{k}{\rho^2} \tag{3-3}$$

and the set (2-5) to (2-8) becomes

$$v' = -\frac{\cos\phi}{\rho^2} + a\cos\beta \tag{3-4}$$

$$\phi' = \left(\frac{1}{\rho^2} - \frac{v^2}{\rho}\right)\frac{\sin\phi}{v} - \frac{a\sin\beta}{v} \tag{3-5}$$

$$\rho' = v\cos\phi \tag{3-6}$$

$$\theta' = \frac{v}{\rho}\sin\phi \tag{3-7}$$

In addition, the energy and momentum are given by

$$k = \rho v\sin\phi \tag{3-8}$$

$$\mathcal{E} = \frac{1}{2}\left(\rho'^2 + \frac{k^2}{\rho^2}\right) - \frac{1}{\rho} = \frac{1}{2}v^2 - \frac{1}{\rho} \tag{3-9}$$

A typical low thrust escape spiral for constant tangential thrust acceleration with $a = 10^{-3}$ is shown in Figure 3-1. The velocity angle ϕ and the orbit eccentricity e are shown as functions of the local thrust acceleration $a\rho^2$ in Figure 3-2 for the same case. These results were obtained by numerical integration of the set (3-4) to (3-7). By the time the vehicle reaches an eccentricity of 0.1, it has spiraled nearly 40 times around the

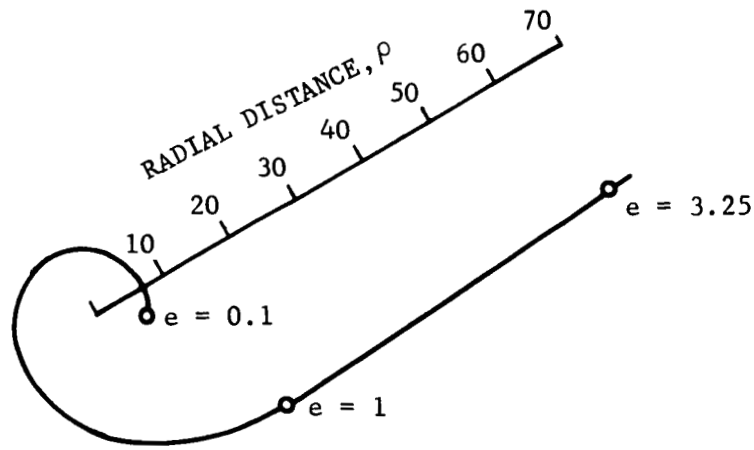

FIGURE 3-1. LAST PORTION OF A LOW THRUST ESCAPE SPIRAL, $\alpha = 10^{-3}$

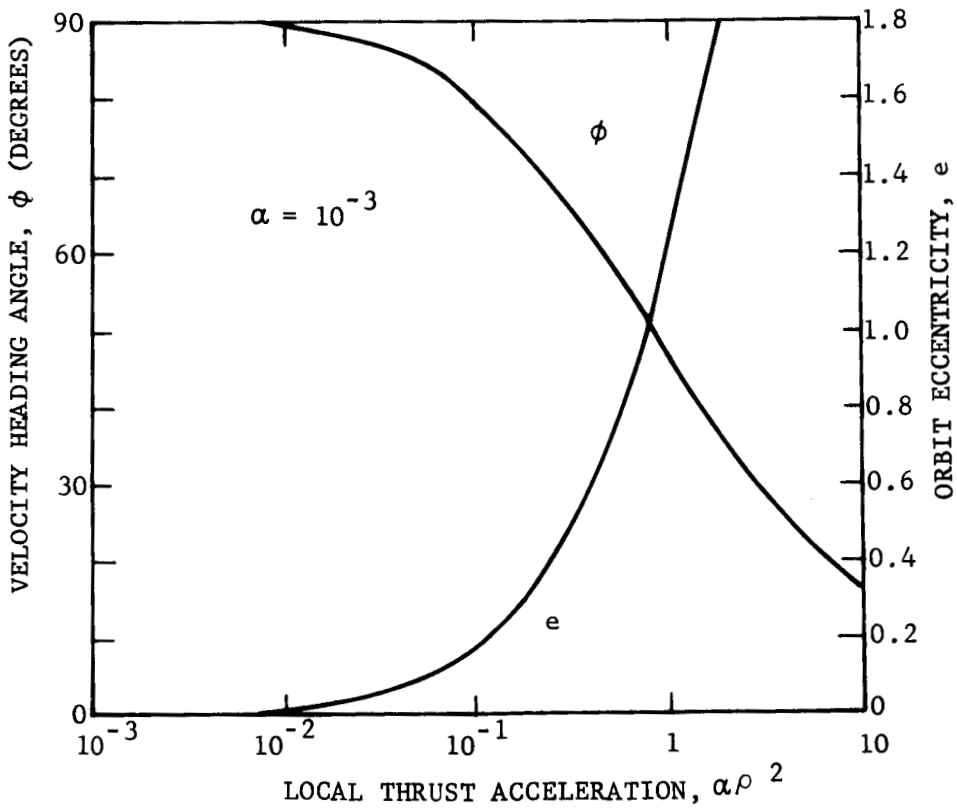

FIGURE 3-2. HEADING ANGLE AND ORBIT ECCENTRICITY

planet with a normalized time $\tau = 620$. In the interval between e = 0.1 and e = 1 (escape), the vehicle makes less than one revolution about the planet; but the additional time increment is 237 so that escape occurs at $\tau = 857$.

Supplementing PERKINS' results [22] with our numerical calculations, conditions at escape were obtained as functions of α. The local thrust acceleration $\alpha\rho^2$ and the normalized velocity $\alpha^{-1/4}v$ are plotted in Figure 3-3, and the characteristic velocity $\alpha\tau$ and velocity angle ϕ are plotted in Figure 3-4. PERKINS was the first to recognize that $\alpha\rho^2$, $\alpha^{-1/4}v$ and ϕ have the same values at escape for $\alpha < 10^{-2}$.

3.2 PERTURBATION SOLUTIONS FOR POWERS OF α^{-1}

ANTHONY [10] obtained perturbation solutions in powers of α^{-1} for five different steering programs:

(1) circumferential thrust

(2) thrust in a fixed direction

(3) tangential thrust

(4) linear off-set from tangential thrust

(5) quadratic off-set from tangential thrust

For this method, the equations of motion (3-1) and (3-2) are cast in the forms

$$\frac{d^2\rho}{d\gamma^2} = \alpha^{-2}\left(\frac{k^2}{\rho^3} - \frac{1}{\rho^2}\right) + \alpha^{-1}\cos\psi \tag{3-10}$$

$$\frac{dk}{d\gamma} = \rho\sin\psi \tag{3-11}$$

where the characteristic velocity $\gamma = \alpha\tau$ is the independent variable. The steering angle ψ satisfies a side condition corresponding to the particular steering program. For the above mentioned steering programs, ρ and k are even functions of α^{-1}. Consequently, the power series solutions are represented as even powers of α^{-1}:

$$\rho = \rho_o + \alpha^{-2}\rho_2 + \alpha^{-4}\rho_4 \tag{3-12}$$

$$k = k_o + \alpha^{-2}k_2 \tag{3-13}$$

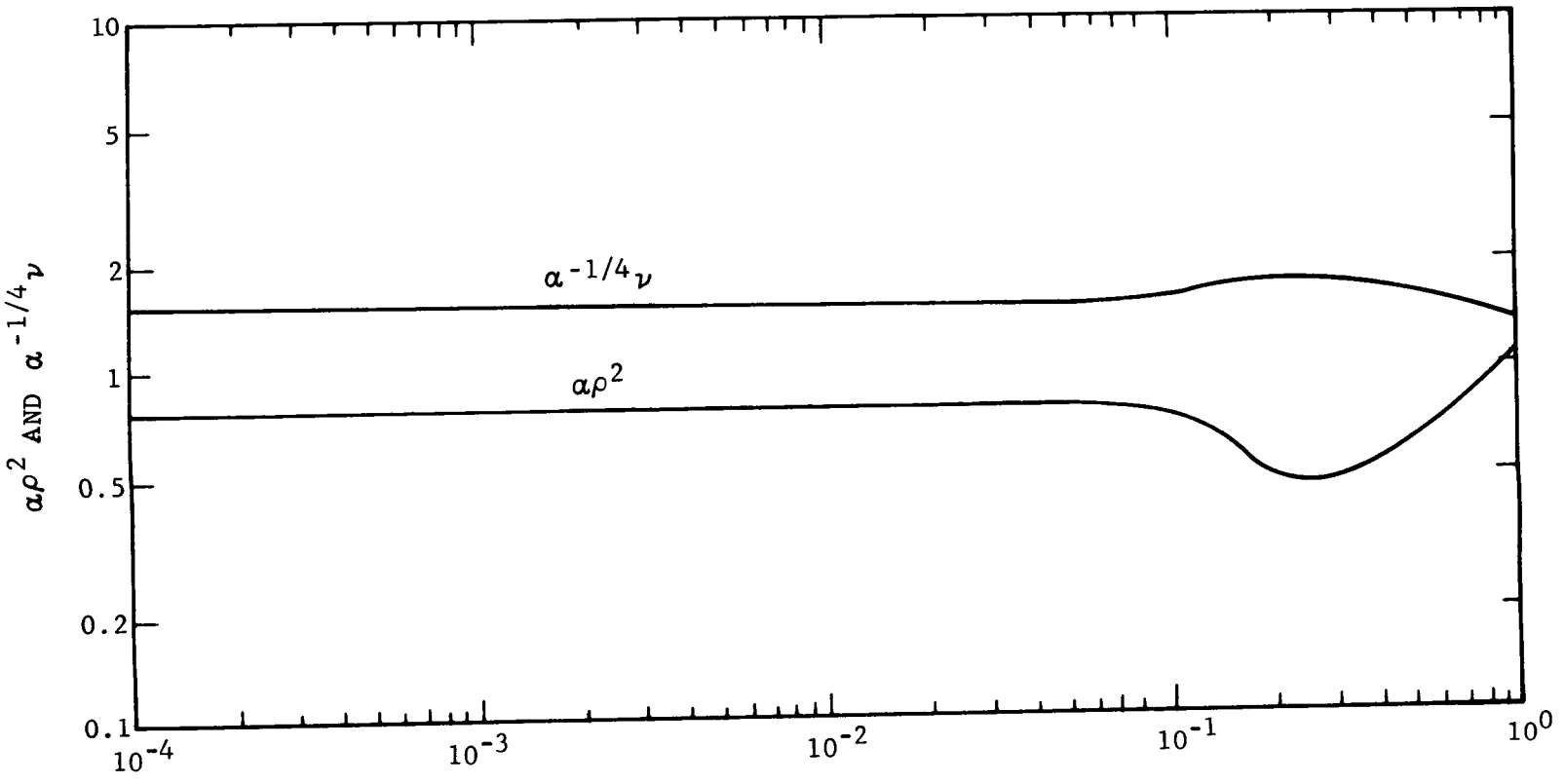

FIGURE 3-3. VELOCITY AND POSITION PARAMETERS AT ESCAPE USING TANGENTIAL THRUST

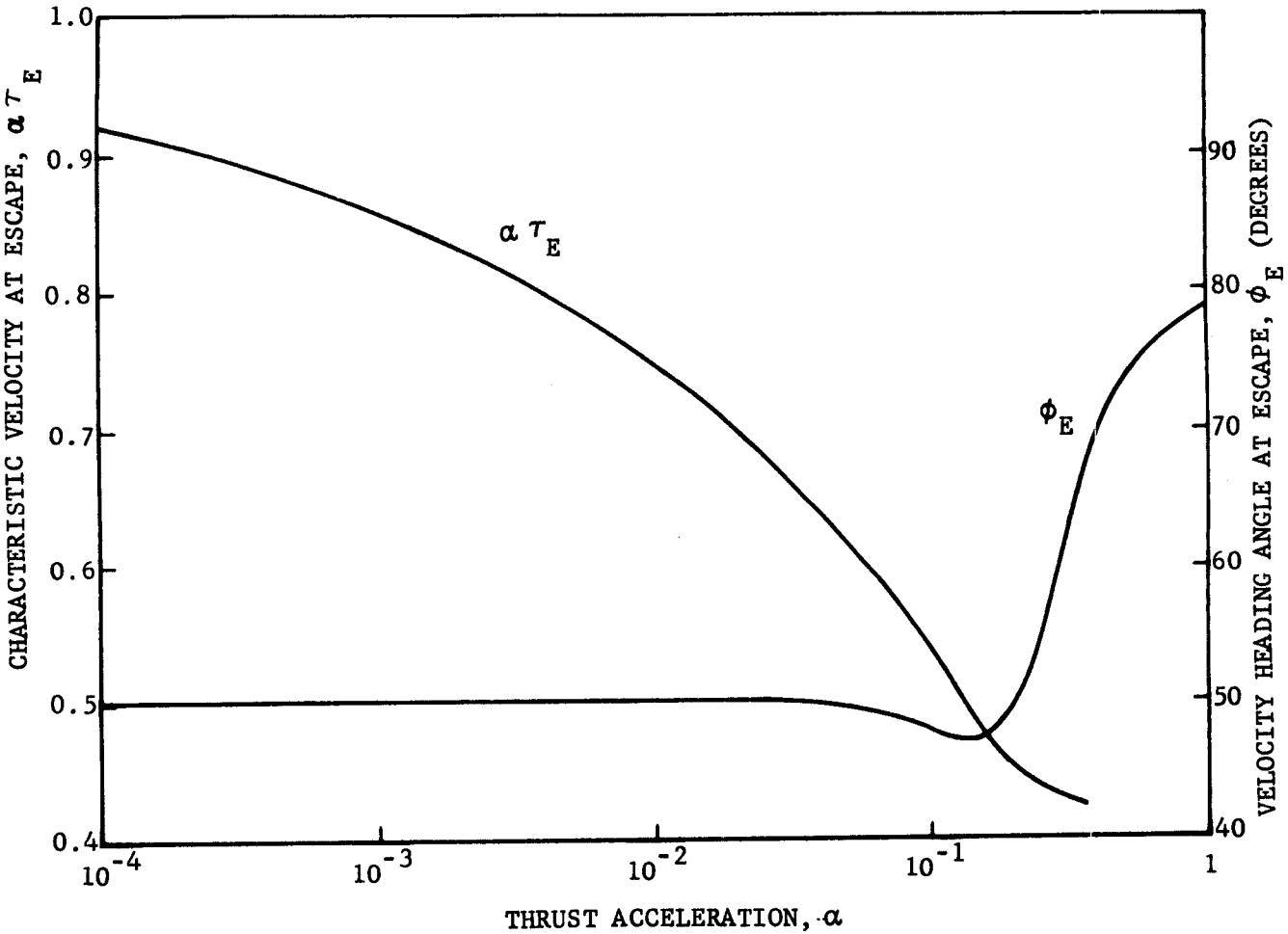

FIGURE 3-4. CHARACTERISTIC VELOCITY AND VELOCITY HEADING ANGLE AT ESCAPE USING TANGENTIAL THRUST

subject to the initial conditions

$$\left.\begin{aligned} &\rho_o = 1, \quad \rho_2 = \rho_4 = 0 \\ &d\rho_o/d\gamma = d\rho_2/d\gamma = d\rho_4/d\gamma = 0 \\ &k_o = 1, \quad k_2 = 0 \end{aligned}\right\} \text{ at } \gamma = 0$$

for a circular orbit.

For circumferential thrust, ANTHONY obtains

$$\rho = 1 + \alpha^{-2}\left(\frac{\gamma^3}{3} + \frac{\gamma^4}{12}\right)$$

$$- \alpha^{-4}\left(\frac{\gamma^5}{3\cdot 4\cdot 5} + \frac{23\gamma^6}{3\cdot 4\cdot 5\cdot 6} + \frac{13\gamma^7}{6\cdot 7\cdot 10} + \frac{13\gamma^8}{6\cdot 7\cdot 8\cdot 10}\right) \qquad (3\text{-}15)$$

Escape is defined by the condition that the energy (3-9) vanish. The predicted characteristic velocity at escape is

$$\alpha\tau_E = 0.414214 + \frac{0.002349}{\alpha^2} - \frac{0.000014}{\alpha^4} \qquad (3\text{-}16)$$

This result is compared in Figure 3-5 to the exact numerical solution for circumferential thrust. The agreement is excellent for $\alpha > 0.2$.

For tangential thrust, the predicted characteristic velocity is somewhat smaller:

$$\alpha\tau_E = 0.414214 + \frac{0.001615}{\alpha^2} - \frac{0.000064}{\alpha^4} \qquad (3\text{-}17)$$

This result was first obtained by BENNY [20] in 1958. It is very close to the optimum steering, second order solution

$$\alpha\tau_E = 0.414214 + \frac{0.001481}{\alpha^2} \qquad (3\text{-}18)$$

predicted by LAWDEN [21] in the same year. Equation (3-17) also shows excellent agreement with the true solution for $\alpha > 0.2$.

Typical values of α for low thrust escape from a near Earth orbit are in the range between 10^{-2} and 10^{-4}. This would suggest that a perturbation solution in powers of α (rather than α^{-1}) be attempted.

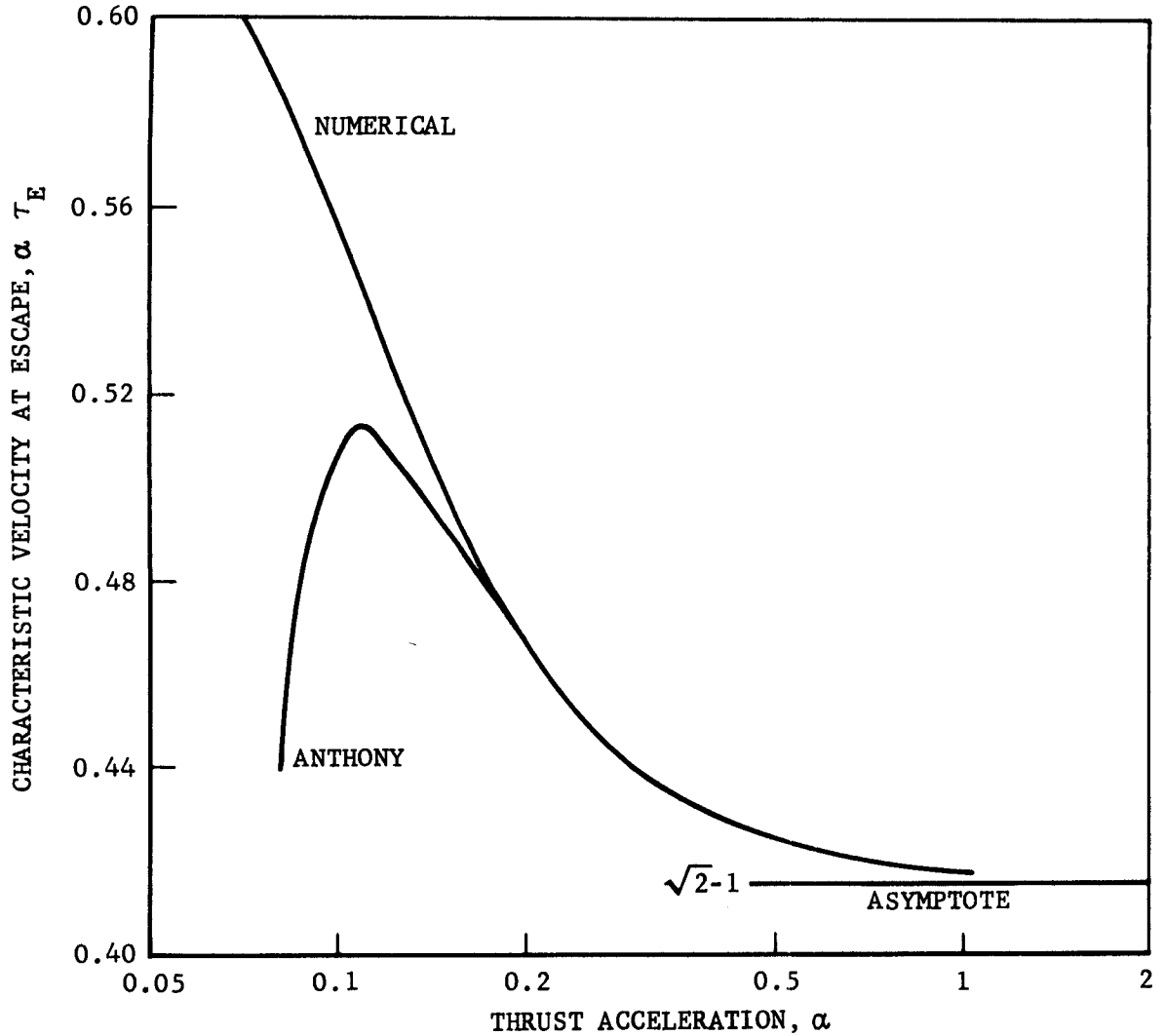

FIGURE 3-5. CHARACTERISTIC VELOCITY AT ESCAPE PREDICTED BY ANTHONY'S SOLUTION FOR CIRCUMFERENTIAL THRUST

3.3 PERTURBATION SOLUTIONS FOR POWERS OF α

LEVIN [2] in 1959 presented a perturbation solution in powers of α for the case of constant circumferential thrust acceleration. This solution was expanded to terms of second order in α. JOHNSON and STUMPF [11,12] extended LEVIN's work to the case when the thrust vector is at any fixed angle ψ relative to the radial direction. On examining this method, it is obvious that time variable functions of ψ could also be accommodated. However, neither LEVIN nor JOHNSON and STUMPF established the range of application of their solutions.

The method of analysis is sketched below. Starting with the differential equations (3-1) and (3-2) subject to the initial conditions

$$\rho = 1, \quad \rho' = 0, \quad k = 1 \quad \text{at} \quad \tau = 0$$

one assumes series solutions for ρ and k in powers of α:

$$\rho = \rho_o + \alpha\rho_1 + \alpha^2 \rho_2 \tag{3-19}$$

$$k = k_o + \alpha k_1 + \alpha^2 k_2 \tag{3-20}$$

Substituting these solutions into (3-1) and (3-2), one obtains a power series in α which must vanish identically in α. Equating coefficients of like powers of α to zero, one finds

$$\rho_o'' = 0 \tag{3-21}$$

$$\rho_1'' + \rho_1 = 2k_1 + \cos\psi \tag{3-22}$$

$$\rho_2'' + \rho_2 = k_1^2 + 2k_2 + 3\rho_1^2 - 6\rho_1 k_1 \tag{3-23}$$

$$k_o' = 0 \tag{3-24}$$

$$k_1' = \sin\psi \tag{3-25}$$

$$k_2' = \rho_1 \sin\psi \tag{3-26}$$

These equations are integrated subject to the initial conditions

$$\left.\begin{aligned} &\rho_o = 1, \quad \rho_o' = 1, \quad k_o = 1 \\ &\rho_i = 0, \quad \rho_i' = 0, \quad k_i = 0 \quad i = 1,2 \end{aligned}\right\} \quad \text{at} \tau = 0 \tag{3-27}$$

Substituting the solutions into (3-19) and (3-20), one gets

$$\begin{aligned} \rho = 1 &+ \alpha[\cos\psi(1-\cos\tau) + 2\sin\psi(\tau - \sin\tau)] \\ &+ \alpha^2\Big[\sin^2\psi(3\tau^2 + 3\tau^2\cos\tau + 5\cos^2\tau + 6\cos\tau + 2\tau\sin\tau - 11) \\ &+ \sin\psi\cos\psi\left(8\tau + \frac{11}{2}\tau\cos\tau - \frac{3}{2}\tau^2\sin\tau - \frac{19}{2}\sin\tau - 4\sin\tau\cos\tau\right) \\ &+ \sin^2\tau - 3\tau\sin\tau - 4\cos\tau + 4\Big] \end{aligned} \tag{3-28}$$

$$\begin{aligned} k = 1 &+ \alpha\sin\psi\tau \\ &+ \alpha^2\left[\sin\psi\cos\psi(\tau - \sin\tau) + \sin^2\psi(\tau^2 + 2\cos\tau - 2)\right] \end{aligned} \tag{3-29}$$

These solutions contain periodic and secular terms. Since secular terms arise in the perturbation method when there are phase shifts in the periodic terms, it is not possible to determine which of the secular terms are characteristics of the true motion.

Consider the special case of radial thrust ($\psi = 0$), which is periodic with no secular phenomena for $\alpha < 1/8$. The exact solution is given by COPELAND [23] with corrections by KARRENBERG [24], and AU[25]. The first order perturbation solution

$$\rho = 1 + \alpha(1 + \cos\tau) \tag{3-30}$$

and the second order perturbation solution

$$\rho = 1 + \alpha(1 + \cos\tau) + \alpha^2(\sin^2\tau - 3\tau\sin\tau - 4\cos\tau + 4) \tag{3-31}$$

are compared to the exact solution in Figure 3-6 for $\alpha < 0$ and in Figure 3-7 for $\alpha > 0$. For $\alpha < 0$, the solutions are plotted to the first minimum for ρ; and for $\alpha > 0$, the solutions are plotted to the first maximum for ρ. Since the true solution is periodic, the motion is completely defined by these segments.

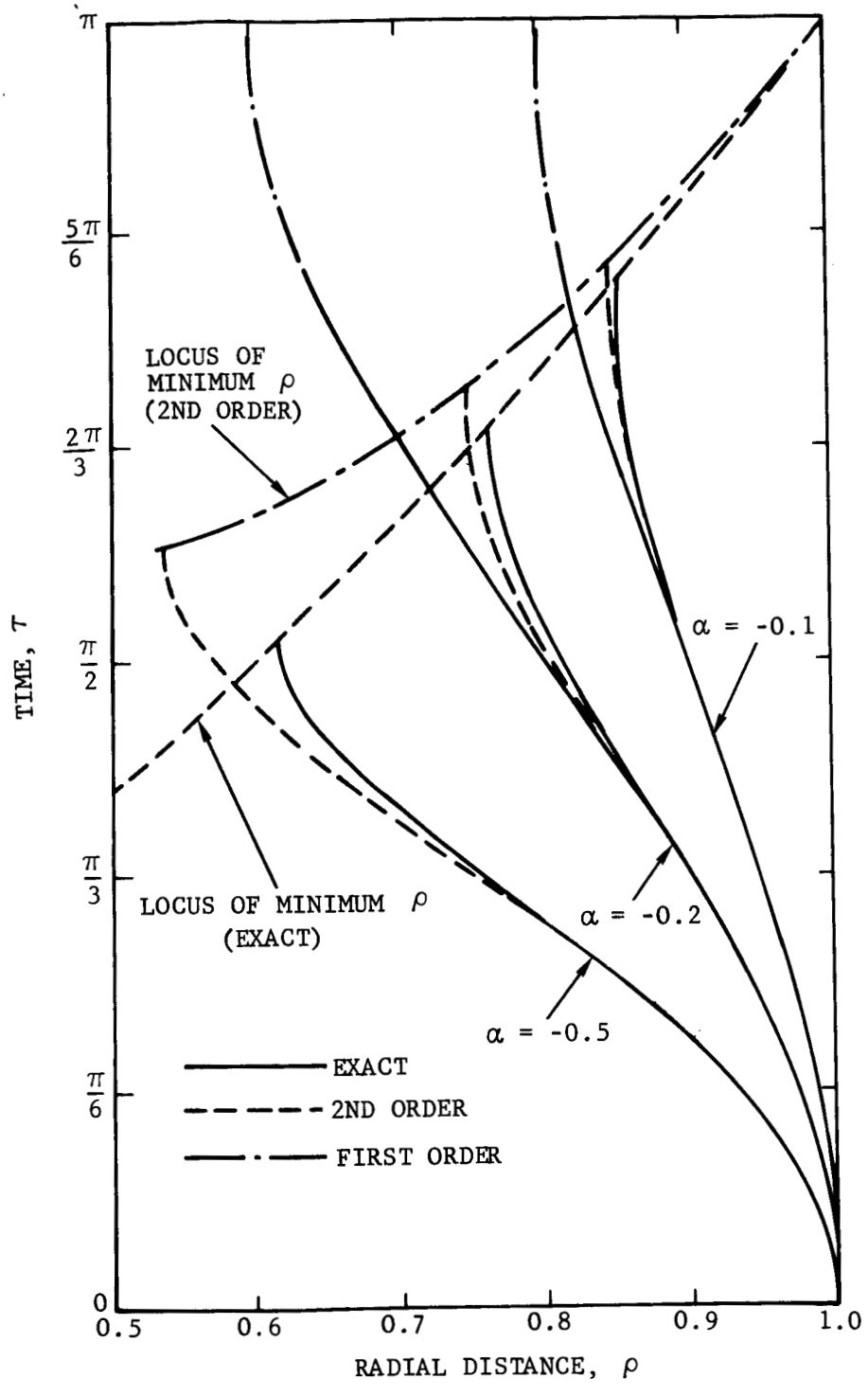

FIGURE 3-6. FIRST AND SECOND ORDER PERTURBATION SOLUTIONS COMPARED T
NUMERICAL SOLUTIONS FOR NEGATIVE RADIAL THRUST

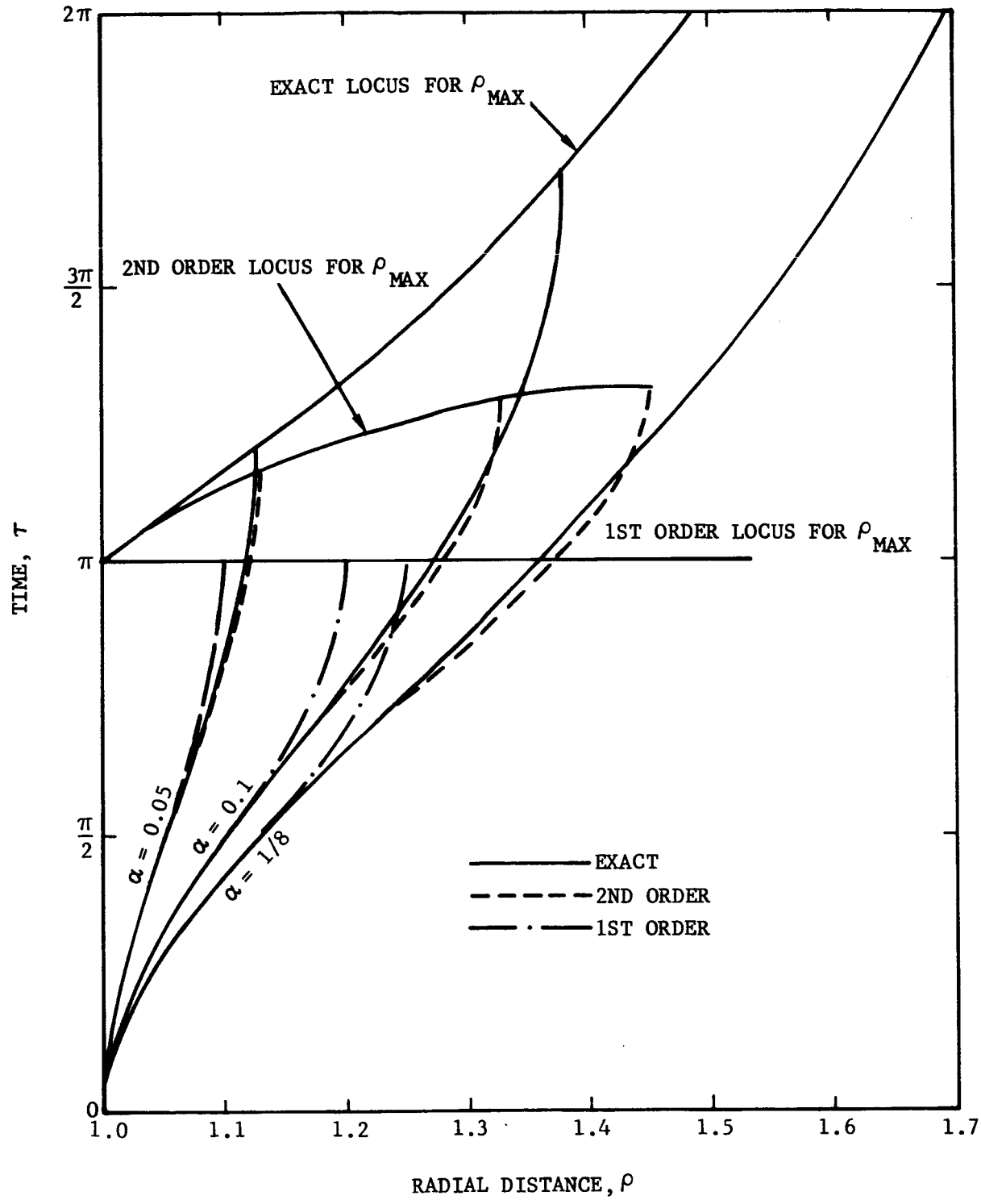

FIGURE 3-7. FIRST AND SECOND ORDER PERTURBATION SOLUTIONS COMPARED TO NUMERICAL SOLUTIONS FOR POSITIVE RADIAL THRUST

The period of the exact solution varies with α; there is a phase shift. The first order solution (3-30), which has no secular terms, does not show the phase shift. On the other hand, the second order solution (3-31) accounts for the phase shift by adding the secular term $-3\alpha^2 \tau \sin \tau$. This incorrectly implies that the motion is secular rather than periodic.

With circumferential thrust ($\psi = \pi/2$) the trajectory is an ever increasing spiral; there is secular phenomena. Both the first and second order solutions for $\psi = \pi/2$ have secular terms. However, one does not know, a priori, if the secular terms are due in part to phase shifts. The perturbation solutions are compared in Figure 3-8 to numerical solutions for different thrust levels. The escape times are also indicated. The second order solutions show good agreement to escape for $\alpha > 0.2$ and poor agreement for smaller α.

Escape, as predicted by the second order solution, is defined by

$$\alpha^2 \left[2 (1 - \cos \tau_E) - \frac{1}{2} \tau_E^2\right] + \alpha \tau_E - \frac{1}{2} = 0 \qquad (3\text{-}32)$$

Solving for the α root with the minus sign, one gets

$$\alpha = \frac{\tau_E - 2 \sqrt{1 - \cos \tau_E}}{\tau_E^2 - 4 (1 - \cos \tau_E)} \qquad (3\text{-}33)$$

This equation was used to generate the curve for $\alpha\tau_E$ shown in Figure 3-9. The range of application is almost identical to ANTHONY's fourth order solution in powers of α^{-1} (see Figure 3-5). This is a disappointing result since a solution valid to escape for $\alpha < 10^{-2}$ was sought.

JOHNSON and STUMPF have suggested that the solution be extended to escape by successively reinitializing the problem. The procedure is impractical if the reference solution must be updated many times before reaching escape. In the limit as the number of times to update increases, the procedure degenerates to "high class" numerical integration.

The first and second order perturbation solutions are compared in Figure 3-10 to the true solutions for $\alpha = 10^{-2}$ and 10^{-3} using circumferential thrust. Local acceleration $\alpha\rho^2$ is plotted as a function of τ. Escape occurs near $\tau = 75$ for $\alpha = 10^{-2}$ and near $\tau = 860$ for $\alpha = 10^{-3}$. Both the first order and second order solutions depart from the true solutions at very small values of τ. The second order solutions exhibit oscillations of increasing amplitude with the first order solution as an approximate lower bound. Using either the first or second order solutions, the reference orbit would have to be updated many times before reaching escape.

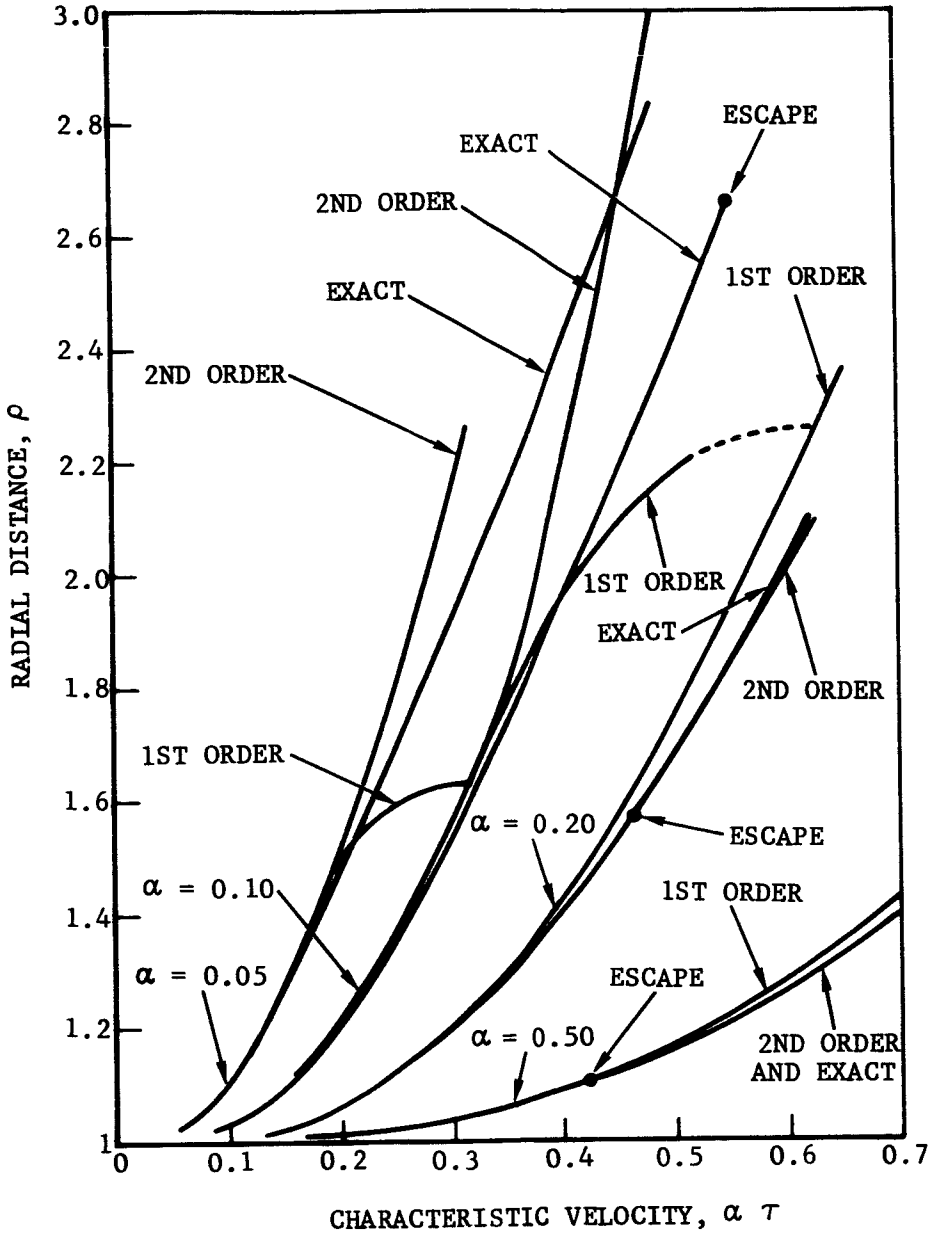

FIGURE 3-8. FIRST AND SECOND ORDER PERTURBATION SOLUTIONS COMPARED TO NUMERICAL SOLUTIONS FOR POSITIVE CIRCUMFERENTIAL THRUST

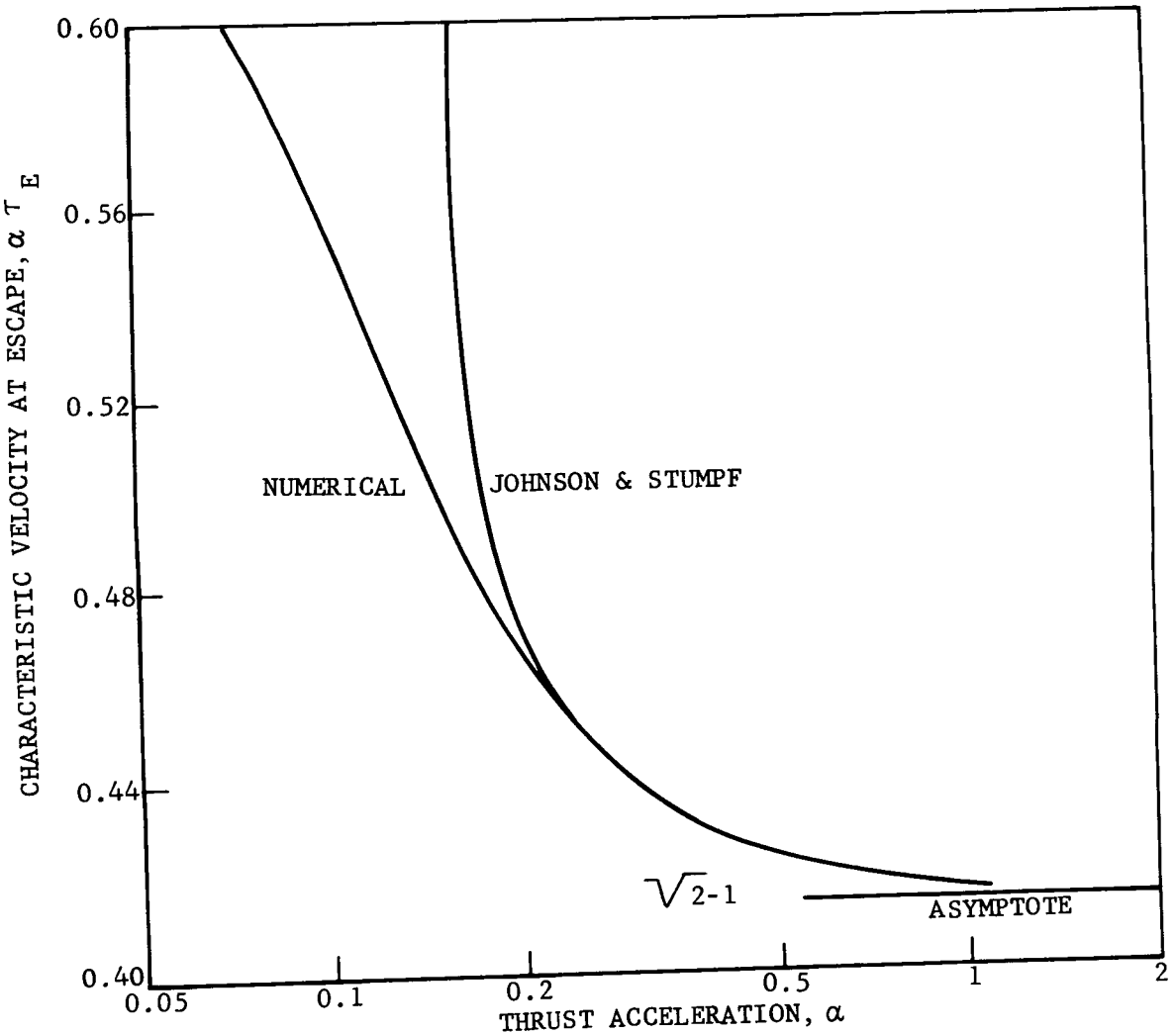

FIGURE 3-9. CHARACTERISTIC VELOCITY AT ESCAPE PREDICTED BY JOHNSON AND STUMPF'S SOLUTION FOR CIRCUMFERENTIAL THRUST

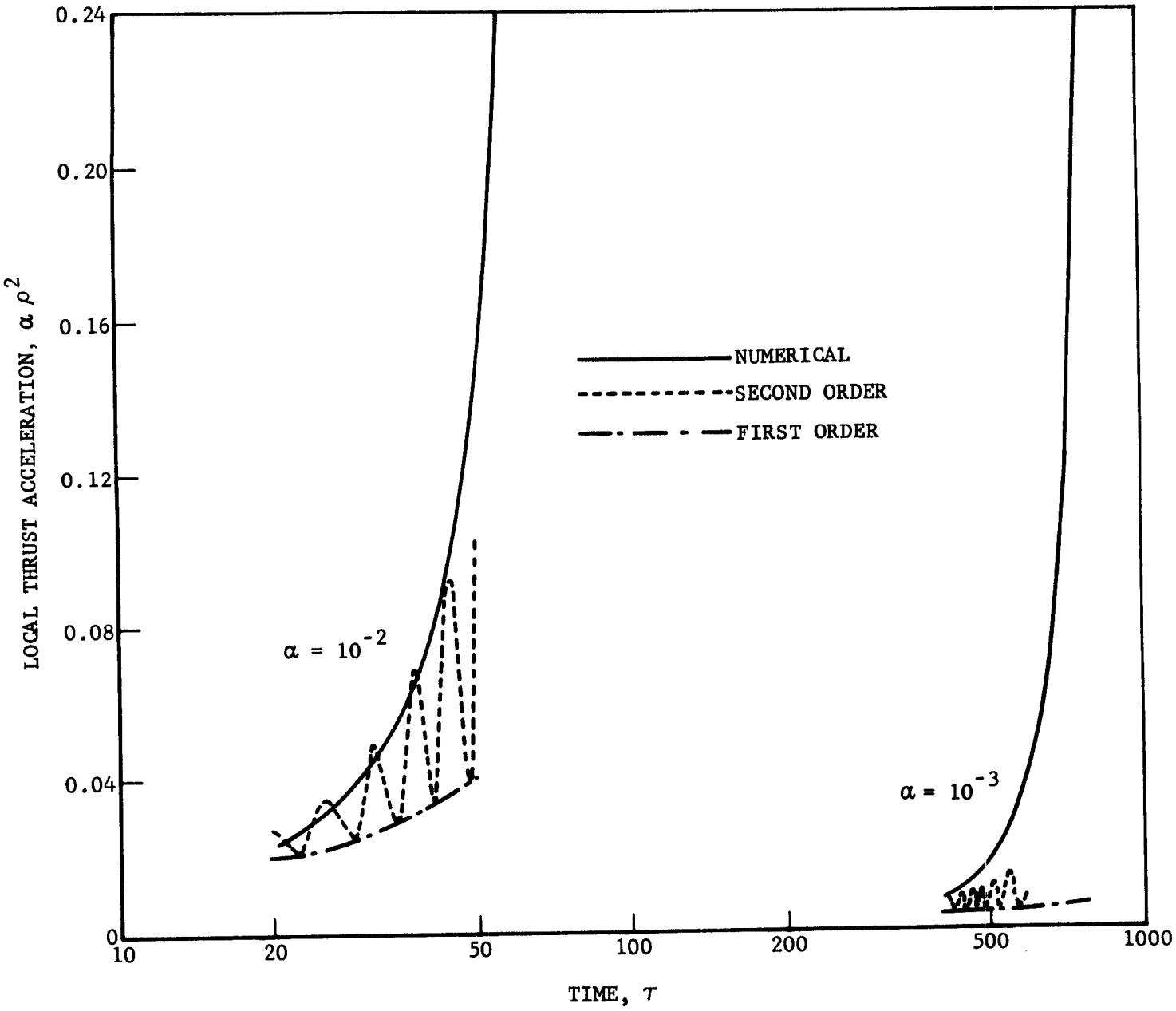

FIGURE 3-10. COMPARISON BETWEEN PERTURBATION AND NUMERICAL SOLUTIONS FOR $\alpha = 10^{-2}$ AND 10^{-3}

Further comparisons were made. The case of $\psi = -\pi/2$ which corresponds to negative circumferential thrust is shown in Figure 3-11. The true solution exhibits an oscillatory decay. The perturbation solutions, first and second order, follow the true solutions to the first local minimums but then depart. The second order solution is more accurate than the first order solution, but it does not extend the range of application.

Comparisons for $\psi = \pi/4$ are shown in Figure 3-12. The results are similar to those shown in Figure 3-8.

Finally JOHNSON and STUMPF in [11] show how their solution could be extended to handle the case of constant thrust for first order changes in mass. In this case, α is a function of τ:

$$\alpha = \frac{\alpha_o}{1 - c\tau} \tag{3-34}$$

where α_o is the initial thrust acceleration and c is a constant which is proportional to the mass flow rate. For small mass changes, c is on the order of α_o. Thus the effect of mass change is second order. The change in ρ due to c is given by

$$\Delta\rho = c\alpha_o \, (\tau^2 + 2\cos\tau - 2) \tag{3-35}$$

The second order perturbation solutions for circumferential thrust with different c and α_o are shown in Figure 3-13. The agreement is about the same as for $c = 0$.

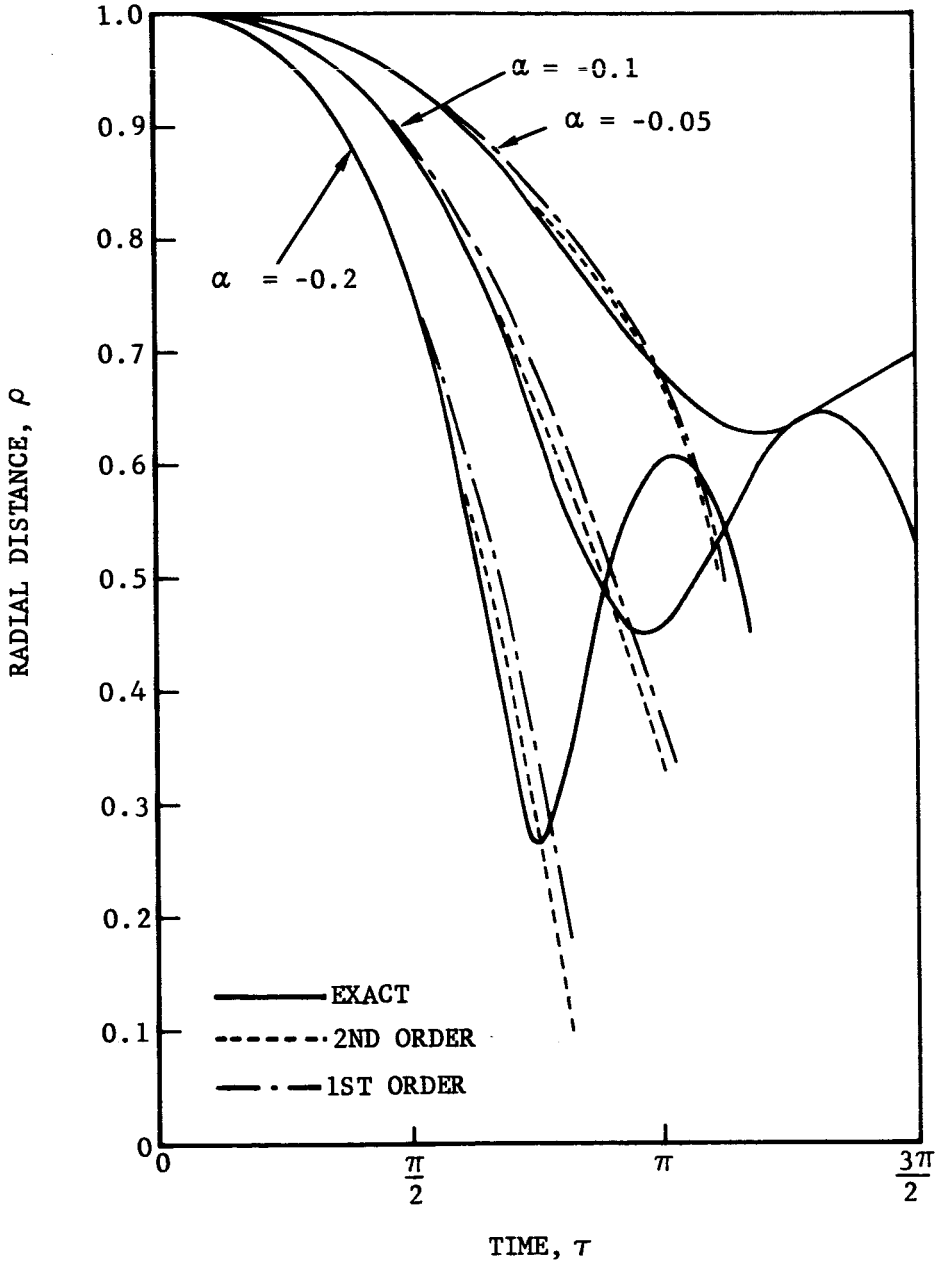

FIGURE 3-11. FIRST AND SECOND ORDER PERTURBATION SOLUTIONS COMPARED TO NUMERICAL SOLUTIONS FOR NEGATIVE CIRCUMFERENTIAL THRUST

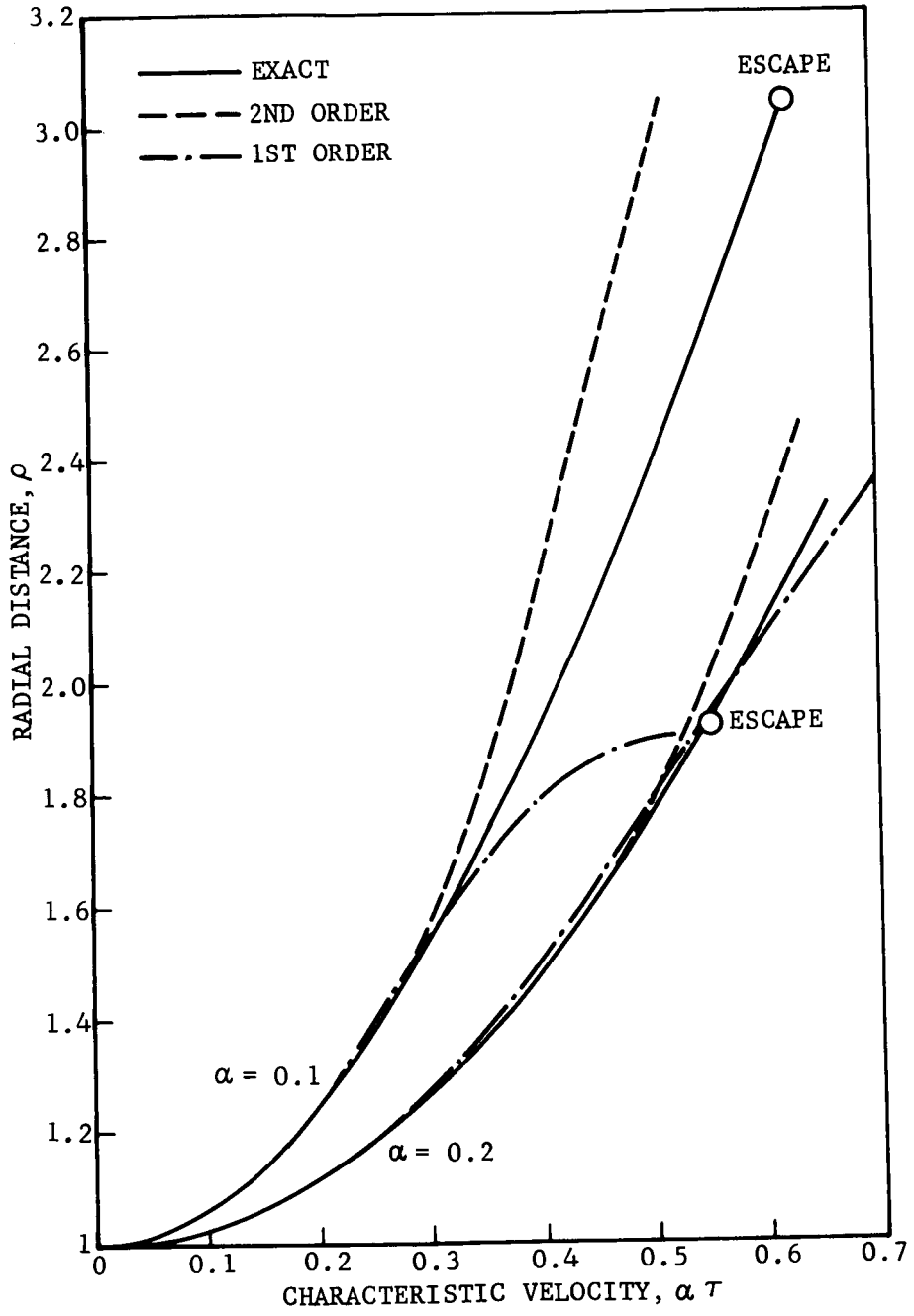

FIGURE 3-12. FIRST AND SECOND ORDER PERTURBATION SOLUTIONS COMPARED TO NUMERICAL SOLUTIONS FOR ψ = 45 DEGREES

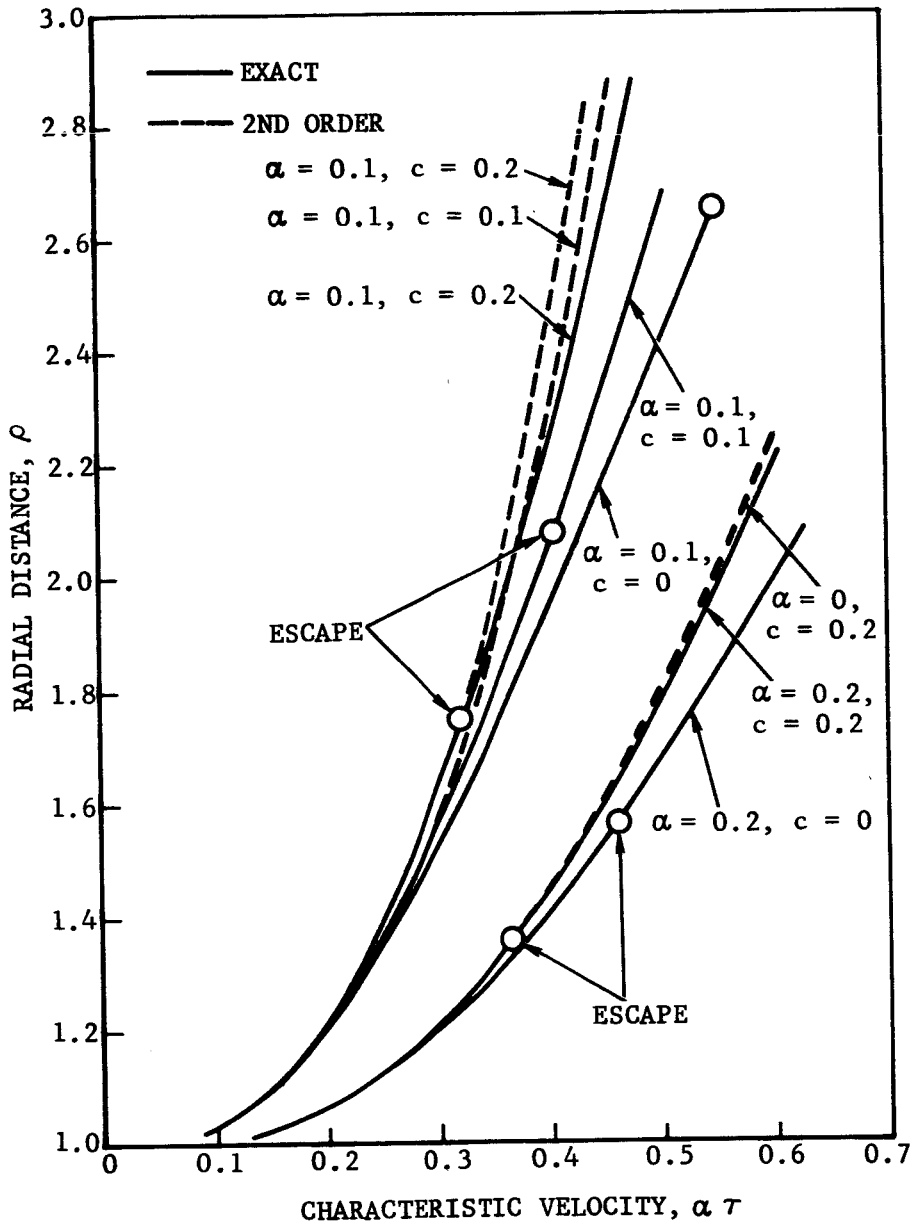

FIGURE 3-13. SECOND ORDER PERTURBATION SOLUTIONS COMPARED TO NUMERICAL SOLUTIONS FOR VARIABLE MASS AND CIRCUMFERENTIAL THRUST

3.4 ASYMPTOTIC METHOD

ZEE [13], and LASS and LORREL [14] used the asymptotic method of KRYLOFF and BOGOLIUBOFF [26] to obtain low thrust trajectories for tangential and circumferential thrust, respectively. The method and its range of application are reviewed below.

To apply the asymptotic method, the set (3-1) to (3-3) must be reformulated with θ as the independent variable and $u = \rho^{-1}$ as a dependent variable. With $w = k^2$ one obtains

$$\frac{d^2u}{d\theta^2} + u = \frac{1}{w} - \frac{\alpha}{wu^2}\left(\cos\psi + \frac{1}{u}\frac{du}{d\theta}\sin\psi\right) \tag{3-36}$$

$$\frac{dw}{d\theta} = \frac{2\alpha}{u^3}\sin\psi \tag{3-37}$$

$$\frac{d\tau}{d\theta} = \frac{1}{u^2\sqrt{w}} \tag{3-38}$$

For $\psi = \pi/2$, (3-36) and (3-37) reduce to

$$\frac{d^2u}{d\theta^2} + u = \frac{1}{w} - \frac{\alpha}{wu^2}\frac{du}{d\theta} \tag{3-39}$$

$$\frac{dw}{d\theta} = \frac{2\alpha}{u^3} \tag{3-40}$$

and for tangential thrust, they reduce to

$$\frac{d^2u}{d\theta^2} + u = \frac{1}{w} \tag{3-41}$$

$$\frac{dw}{d\theta} = \frac{2\alpha}{u^2\sqrt{\left(\frac{du}{d\theta}\right)^2 + u^2}} \tag{3-42}$$

When $\alpha = 0$, the solutions to (3-36) and (3-37) are

$$u = \frac{1}{b} + A\cos(\theta - \chi) \tag{3-43}$$

where w, A, and χ are constants. The quantity Aw corresponds to the orbit eccentricity e.

ZEE [13] determined the changes in w, A, and χ for constant tangential thrust acceleration. In carrying out his solution he dropped terms of order e^2, assuming e remains small. With this assumption, the differential equations for w, A, and χ can be written as

$$\frac{dw}{d\theta} = 2\alpha w^3 (1 - 3Aw \cos \gamma) \tag{3-44}$$

$$\frac{dA}{d\theta} = 2\alpha w (1 - 3Aw \cos \gamma) \cos \gamma \tag{3-45}$$

$$\frac{d\chi}{d\theta} = 2\alpha \frac{w}{A} (1 - 3Aw \cos \gamma) \sin \gamma \tag{3-46}$$

where $\gamma = \theta - \chi$. For small α, the derivatives are replaced by their average values

$$\left\langle \frac{dw}{d\theta} \right\rangle = \frac{1}{2\pi} \int_0^{2\pi} \frac{dw}{d\theta} d\gamma = 2\alpha w^3 \tag{3-47}$$

$$\left\langle \frac{dA}{d\theta} \right\rangle = \frac{1}{2\pi} \int_0^{2\pi} \frac{dA}{d\theta} d\gamma = -3\alpha A^2 w^2 \tag{3-48}$$

$$\left\langle \frac{d\chi}{d\rho} \right\rangle = \frac{1}{2\pi} \int_0^{2\pi} \frac{d\chi}{d\theta} d\gamma = 0 \tag{3-49}$$

where A, w, and χ are treated as constants under the integrals.

With initial conditions corresponding to a circular orbit, ZEE obtains

$$\frac{1}{\rho} = \sqrt{1 - 4\alpha\theta} (1 + e \sin \theta) \tag{3-50}$$

where the eccentricity e is given by

$$e = 2\alpha (1 - 4\alpha\theta)^{1/4} \tag{3-51}$$

For $\alpha < 10^{-2}$, the solution for ρ can be approximated by

$$\rho = \frac{1}{\sqrt{1 - 4\alpha\theta}} \tag{3-52}$$

which defines a spiral with ever increasing amplitude. Integrating (3-38) using (3-52) one obtains

$$\tau = \int_{\theta_o} \frac{d\theta}{(1 - 4\alpha\theta)^{3/4}} = \frac{1}{\alpha}\left[1 - (1 - 4\alpha\theta)^{1/4}\right] \tag{3-53}$$

which together with (3-52) provides

$$\rho = \frac{1}{(1 - \alpha\tau)^2} \tag{3-54}$$

Equation (3-54) was used to obtain the plots of local thrust acceleration $\alpha\rho^2$ shown in Figure 3-14. The asymptotic solutions are accurate to $\alpha\rho^2 = 0.1$ and 0.05 for $\alpha = 10^{-2}$ and 10^{-3}, respectively. As $\alpha\rho^2$ increases beyond these values, the eccentricity rapidly increases (see Figure 3-2). These results are immeasurably better than those obtained using the perturbation method (see Figure 3-10). However, they are not applicable to escape.

Recall that ZEE assumed e remains small. LASS and LORREL [14] considered the case of circumferential thrust without making any assumptions on e. Their analysis shows that the average change in e is given by

$$\left\langle \frac{de}{d\theta} \right\rangle = -\frac{3\alpha w^2 e}{2(1 - e^2)^{3/2}} \tag{3-55}$$

This result indicates that e decreases with increasing θ for positive α, and gives no hint of the actual phenomena. Hence their solution is no more accurate than ZEE's at least for positive α.

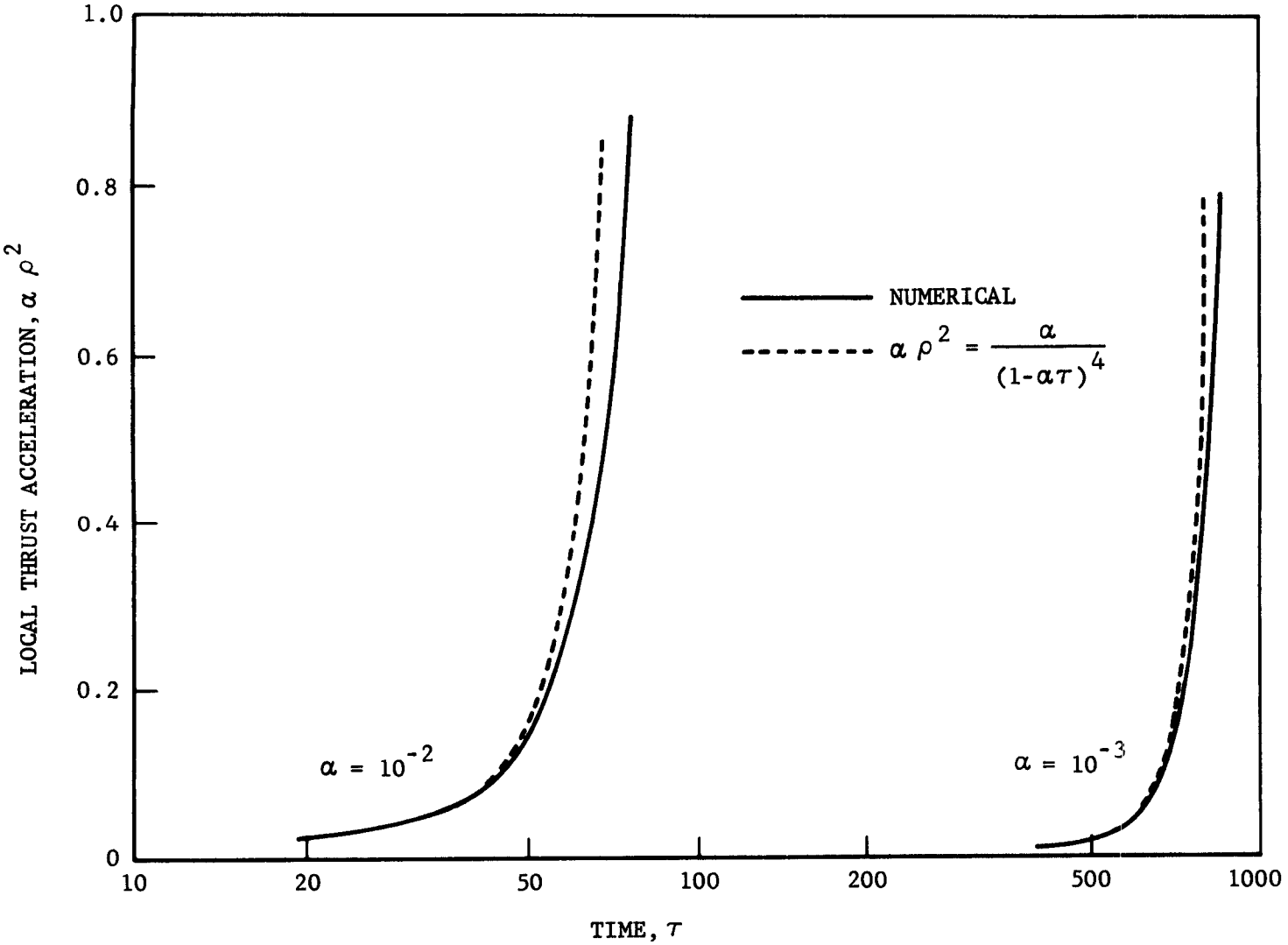

FIGURE 3-14. COMPARISON BETWEEN ASYMPTOTIC AND NUMERICAL SOLUTIONS FOR $\alpha = 10^{-2}$ AND 10^{-3}

SECTION 4

GUIDANCE LAWS FOR THE ESCAPE AND CAPTURE PHASES

4.1 ESCAPE PHASE

The principal error source during the escape phase is the uncertainty in the thrust acceleration level. Several revolutions may pass before the thrust level can be determined to the desired accuracy. A small error $\Delta\alpha$ in α, if allowed to persist, will lead to errors in position, velocity, and time at escape. These errors can be estimated by the equations:

$$\frac{\Delta\tau}{\tau} = -\frac{4}{3}\frac{\Delta\alpha}{\alpha} \tag{4-1}$$

$$\frac{\Delta\rho}{\rho} = -2\frac{\Delta\alpha}{\alpha} \tag{4-2}$$

$$\frac{\Delta v}{v} = 4\frac{\Delta\alpha}{\alpha} \tag{4-3}$$

$$\frac{\Delta\phi}{\phi} = 0 \tag{4-4}$$

$$\frac{\Delta\theta}{\theta} = -4\frac{\Delta\alpha}{\alpha} \tag{4-5}$$

The first four relations were derived from conditions set down by PERKINS [22], and the last relation was derived from (3-53).

The nominal escape conditions for $\alpha = 10^{-3}$ are $\tau = 857$, $\rho = 27.8$, $v = 0.268$, $\phi = 50.8$ degrees and $\theta = 40$ revolutions. The changes in these parameters for

a one percent change in α are all small, and with the exception of $\Delta\theta$ are unimportant. Though $\Delta\theta$ is only 0.4 revolutions, it represents a large directional error in the departure asymptote. This is illustrated in Figure 4-1 where the nominal path departs along an asymptote defined by Φ and the off-nominal path departs along an asymptote 144 or 216 degrees removed from the nominal, depending on the viewpoint.

It is evident that if one waits until the last revolution to correct Φ large errors in ρ, v, and τ at escape will result. BATTIN and MILLER [15] suggest that the thrust acceleration be varied shortly before the last revolution to correct Φ. This scheme, while theoretically correct, suffers in that very small corrective thrusts must be measured and monitored.

The recommended scheme is to simply turn the thrust off for a short interval before the last revolution. It is important that the eccentricity be small otherwise additional errors in ρ, v, and ϕ result. The coast time interval $\Delta\tau$ is related to the desired angular correction $\Delta\theta$ by the equation

$$\Delta\tau = \rho^{3/2} \Delta\theta \tag{4-6}$$

where ρ is the mean radius of the coast orbit. For the case shown in Figure 4-1, ρ is 5.58 at the end of the 38th revolution. If the correction $\Delta\theta$ = 216 degrees (or 3.79 radians) were made at this time, $\Delta\tau$ would be 41.5. The nominal escape time τ is 857. Thus $\Delta\tau$ represents a 5 percent time error, which converts to an error in the target planet lead angle θ_L at the start of the interplanetary phase.

4.2 CAPTURE PHASE

Under nominal conditions, the capture trajectory is simply the reverse of an escape trajectory which commences at the desired circular orbit about the target planet and which uses tangential thrust. The escape parameters ρ_E, v_E, ϕ_E are given in Figures 3-3 and 3-4 for different α. The nominal capture trajectory commences at

$$\rho_{c_o} = \rho_E, \qquad v_{c_o} = v_E, \qquad \phi_{c_o} = \phi_E + \pi \tag{4-7}$$

and uses negative tangential thrust, that is, $\beta = \pi$.

Capture is defined by the condition

$$\frac{1}{2} v_c^2 - \frac{1}{\rho_c} = 0 \tag{4-8}$$

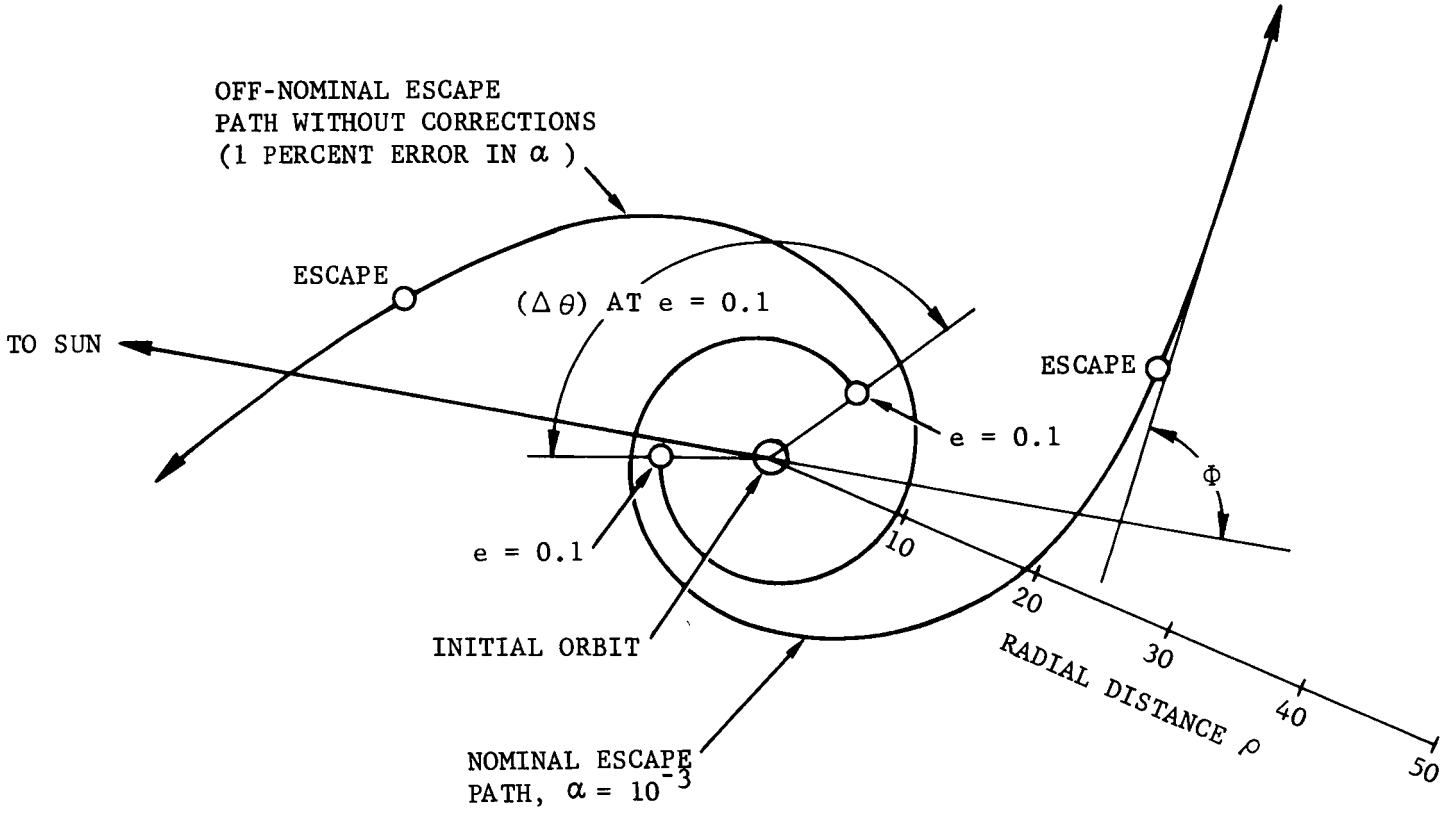

FIGURE 4-1. ESCAPE ASYMPTOTES WITH 1 PERCENT THRUST ACCELERATION DIFFERENCE

Errors develop when the actual capture parameters ρ_c, v_c, and ϕ_c are different than the nominal capture values ρ_{c_o}, v_{c_o} and ϕ_{c_o}. Such differences are the residual errors of the interplanetary transfer phase. Since v_c is related to ρ_c by (4-8), only ρ_c and ϕ_c need to be specified.

Tangential thrust in the negative direction is only acceptable when starting at the nominal capture values. For off-nominal capture values, tangential thrust does not circularize the capture trajectory. Unlike the escape problem, the capture problem cannot be disposed by simply turning the thrust off and on, or by varying the thrust magnitude over a small range. Rather the thrust direction itself must be controlled to achieve the desired terminal conditions.

BATTIN and MILLER [15] have formulated one solution to the capture problem. The following features characterize their method:

1. The scheme employs variable thrust acceleration with an upper limit. More often than not they ride this upper limit. It is not obvious whether their scheme would work if the thrust acceleration were fixed.

2. The scheme does not depend on either continuous or intermittent solution of the two body orbit. In other words, it is not an explicit guidance mechanization.

3. The scheme uses stored values of the thrust acceleration vector and the velocity vector as functions of the radial distance along a pseudo-reference orbit. This data together with instantaneous velocity and position data are used to determine the steering direction.

4. The scheme steers along the pseudo-reference orbit only in the absence of errors. The capture trajectory is not optimal when there are errors, but the characteristic velocity penalties may be small.

4.3 A NEW TERMINAL GUIDANCE SCHEME

The objective was to formulate a guidance law for the capture phase which does not depend on the explicit solution to the equations of motion or comparison to any reference trajectory. The scheme would simultaneously reduce the semi-major axis a and the eccentricity e of the instantaneous KEPLER ellipse. Now a and e are related to the normalized energy $\mathcal{E}$ and k by

$$a = -\frac{1}{2\mathcal{E}}, \qquad e = \sqrt{1 + 2\mathcal{E}k^2}$$

The capture phase commences at $\mathcal{E} = 0$ and is completed at $\mathcal{E} = -1/2$. If the orbit is to be circular at $\mathcal{E} = -1/2$, k^2 must be unity. With negative tangential thrust, both the energy and momentum decrease, even when the latter is less than 1.

The deficiency of negative tangential steering can be eliminated by providing a component of normal acceleration which increases the angular momentum. This is accomplished by the steering law

$$\beta = \pi + K\left(\frac{\pi}{2} - \phi\right) \tag{4-9}$$

with the constraint

$$\frac{\pi}{2} \leq \beta \leq \frac{3\pi}{2} \tag{4-10}$$

K is the control gain, a constant in this case. When K = 0 the thrust is in the negative tangential direction. The correction angle $K(\pi/2 - \phi)$ introduces a normal component of thrust which increases the angular momentum whenever the velocity vector is inclined to the circumferential direction. The constraint (4-10) is imposed so that the thrust will never cause the energy to increase.

The steering law (4-9) was evaluated for several combinations of K and capture parameters ρ_c and ϕ_c. Two typical runs with K = 1 and K = 5 are shown in Figure 4-2 for $\alpha = 10^{-3}$ (normalized on the desired circular orbit $\rho = 1$). The assumed capture conditions are $\rho_c = 40$ and $\phi_c = 147$ degrees compared to the nominal values $\rho_{c_o} = 27.8$ and $\phi_{c_o} = 129.2$ degrees. With K = 1, ρ converges to 1 in an oscillatory fashion. The oscillation is a measure of the orbit eccentricity. When $\mathcal{E}$ reaches -1/2 at $\tau = 990$, the eccentricity is 0.43, which is too large. With a large gain, K = 5, the oscillation in ρ disappears, but now $\mathcal{E}$ reaches -1/2 at $\tau = 1200$. Thus there is a trade-off between the final orbit eccentricity and the characteristic velocity required to reach $\mathcal{E} = -1/2$.

Further examination of Figure 4-2 reveals that the large gain is probably too large at the beginning (the hump in ρ), and the small gain is too small toward the end (the oscillation in ρ). We concluded that the guidance scheme could be improved by employing a variable gain K, one which increases as $\mathcal{E}$ decreases.

Three variable steering gains

$$K = K_{1/2}\left(|\mathcal{E}| - \mathcal{E}\right)^{1/2} \tag{4-11}$$

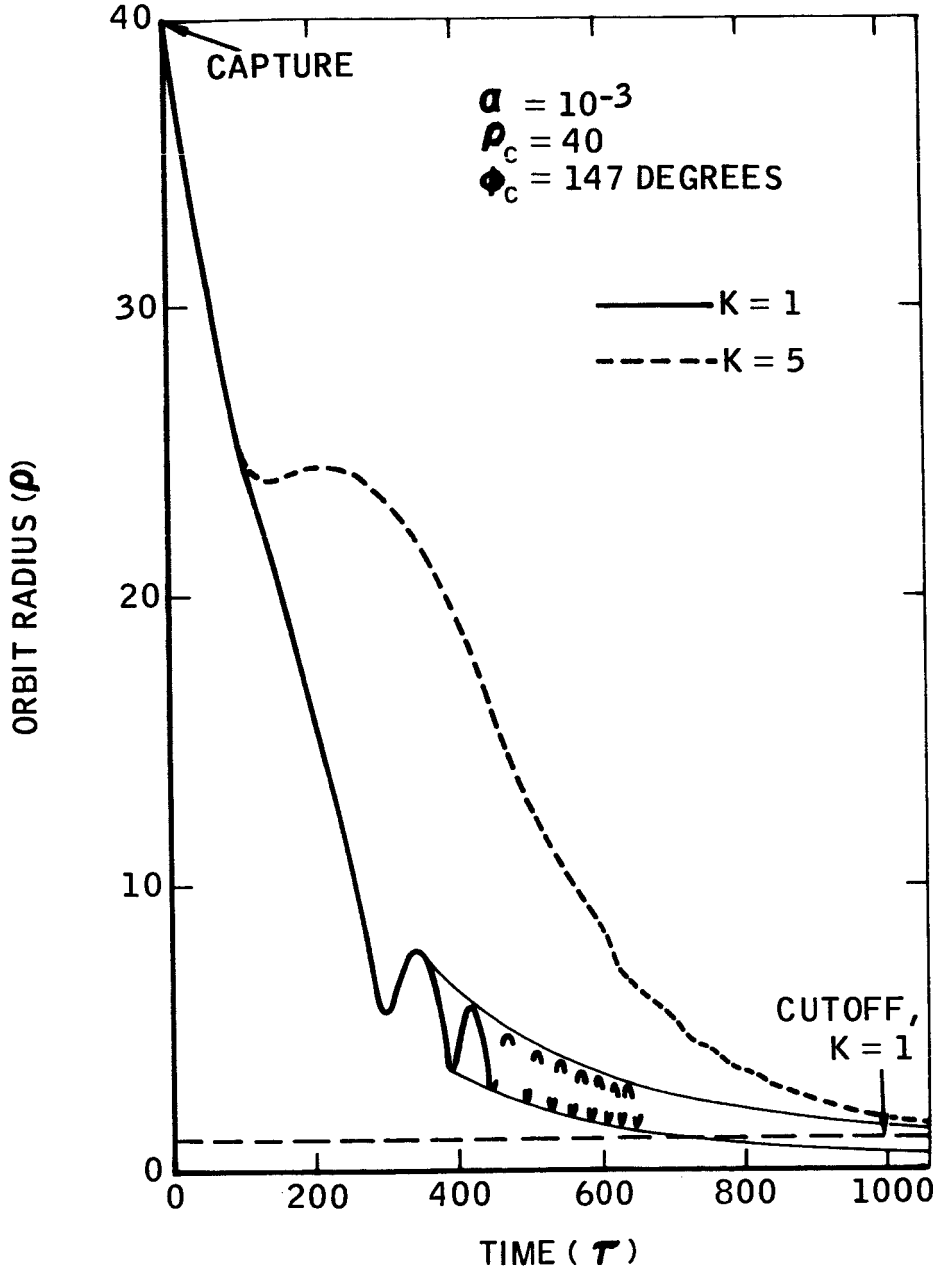

FIGURE 4-2. ORBIT RADIUS WITH CONSTANT STEERING GAINS

$$K = K_1 (|\mathcal{E}| - \mathcal{E}) \tag{4-12}$$

$$K = K_2 (|\mathcal{E}| - \mathcal{E})^2 \tag{4-13}$$

were tested for ranges of the gain coefficients $K_{1/2}$, K_1, and K_2. $\mathcal{E}$ is positive before capture, zero at capture and negative thereafter. The argument $|\mathcal{E}| - \mathcal{E}$ is therefore zero before capture and approaches 1 as $\mathcal{E}$ approaches -1/2. Different values of the gains $K_{1/2}$, K_1, and K_2 are evaluated in Figures 4-3, 4-4, and 4-5, respectively for the same α and capture conditions as used for the runs in Figure 4-2. The best results for this particular set of conditions were obtained with $K_1 = 30$. The terminal condition $\mathcal{E} = -1/2$ was reached at $\tau = 955$ compared to $\tau = 1200$ for a constant gain K of 5. Furthermore, the orbit eccentricity at this point is essentially zero ($e = 4 \times 10^{-4}$). In subsequent studies, only the linear steering gain K_1 was considered.

For nominal capture conditions, the minimum characteristic velocity $\alpha\tau$ is 0.857 for $\alpha = 10^{-3}$. The minimum value is achieved by steering to $\beta = \pi$. The minimum $\alpha\tau$ for off-nominal capture conditions has never been determined. The proposed steering law

$$\beta = \pi + K_1 (|\mathcal{E}| - \mathcal{E}) \left(\frac{\pi}{2} - \phi\right) \tag{4-14}$$

$$\frac{\pi}{2} \leq \beta \leq \frac{3\pi}{2} \tag{4-10}$$

is not optimal even for the nominal capture conditions. This contrasts with BATTIN and MILLER's terminal guidance scheme which is optimum in the absence of errors. The efficiency of the proposed steering law may be assessed from Figures 4-6 and 4-7. In the first figure, $\alpha\tau$ is plotted as a function of ϕ_c for the nominal ρ_{c_o} and in the second figure $\alpha\tau$ is plotted as a function of ρ_c for the nominal ϕ_{c_o}. Two gain coefficients $K_1 = 10$ and 30 are used. The smaller gain is more efficient for small errors and less efficient for large errors. In the absence of errors $\alpha\tau$ is 0.932 for $K_1 = 30$ and 0.874 for $K_1 = 10$, which represent inefficiencies of 9 and 2 percent respectively when compared to the optimum value. Thus if one knew the errors were going to be small, a small K_1 could be used, and vice versa.

Figure 4-8 is a plot of the characteristic velocity contours as functions of ρ_c and ϕ_c for $\alpha = 10^{-3}$ and $K_1 = 30$. The contours are symmetric about $\phi_c = 180$ degrees, the straight-in approach, indicating that $\alpha\tau$ is independent of the direction of rotation about the plant. In all the cases shown, the final orbit eccentricity is less than 0.02. The proposed terminal guidance scheme can accommodate large errors in ρ_c and ϕ_c. However, for ρ_c as large as 60, cases were found which did not converge. In these cases, the velocity was reduced to zero at a point where $\alpha\rho^2$ was larger than one, indicating that the thrust acceleration was larger than the planet gravity. As a result, the thrust vector pinwheels around and opposes any velocity increment.

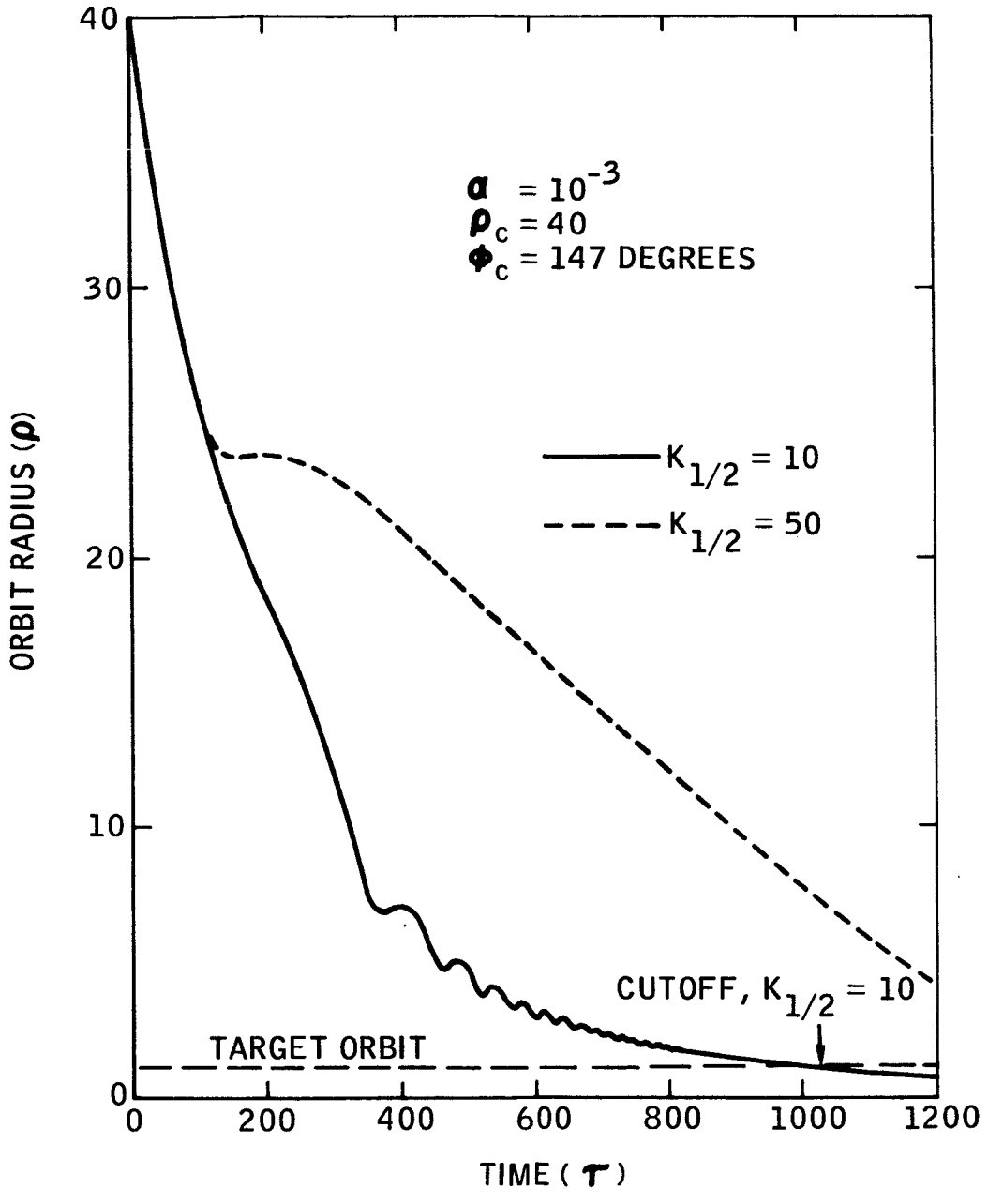

FIGURE 4-3. ORBIT RADIUS WITH THE "SQUARE ROOT" STEERING GAIN, $K_{1/2}$

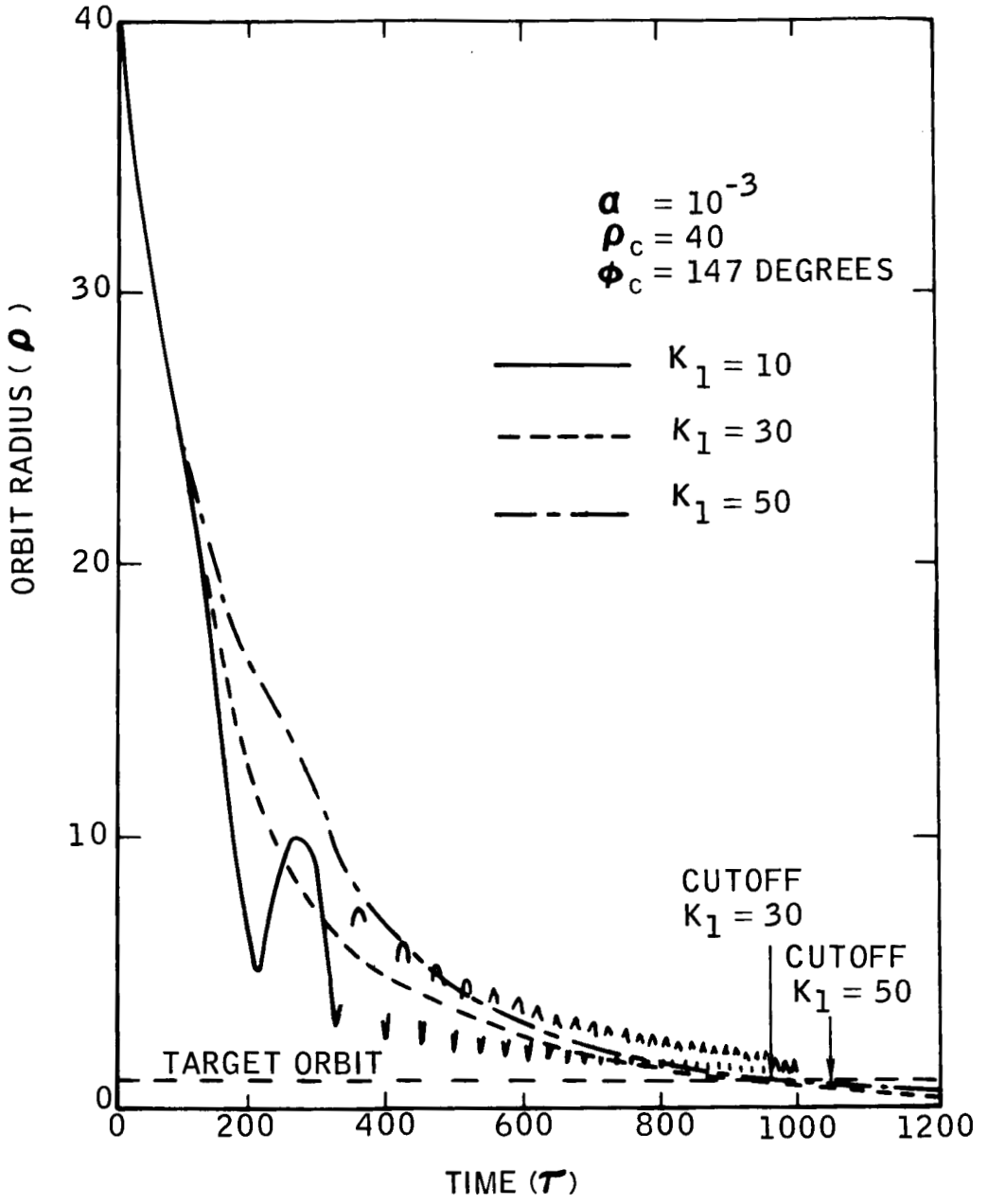

FIGURE 4-4. ORBIT RADIUS WITH THE LINEAR STEERING GAIN K_1

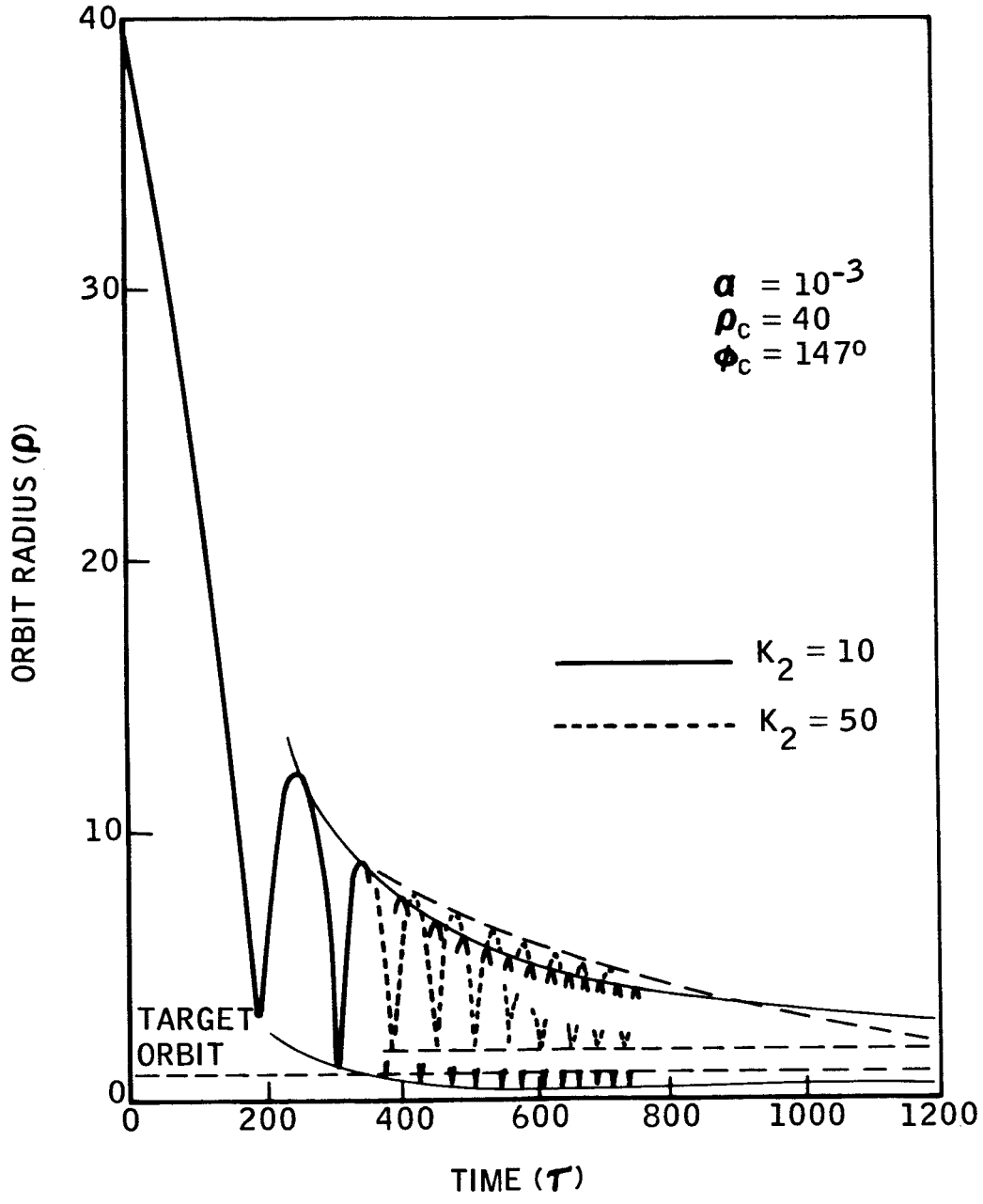

FIGURE 4-5. ORBIT RADIUS WITH THE QUADRATIC STEERING GAIN, K_2.

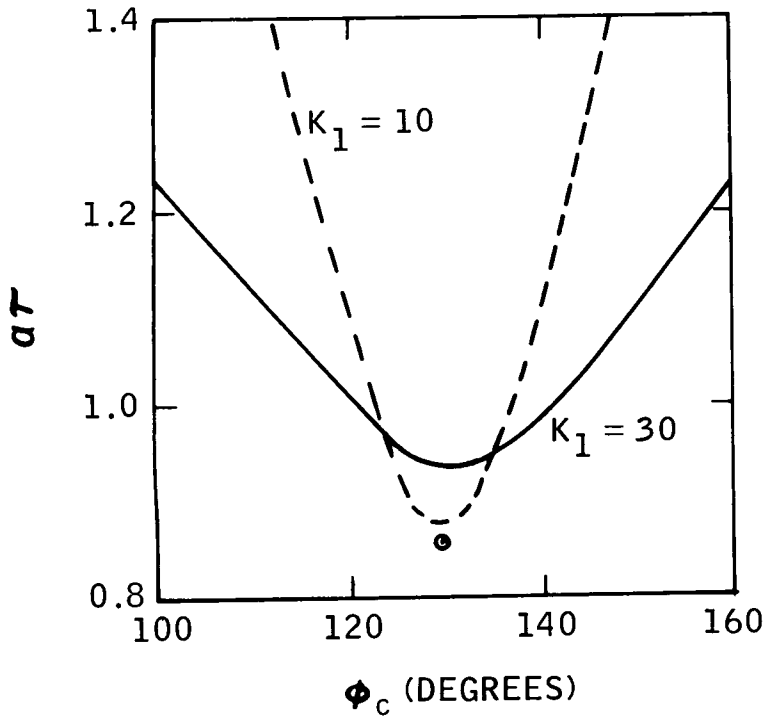

FIGURE 4-6. CHARACTERISTIC VELOCITY AS A FUNCTION OF ϕ_c FOR $\rho_{c_0} = 27.8$ AND $a = 10^{-3}$

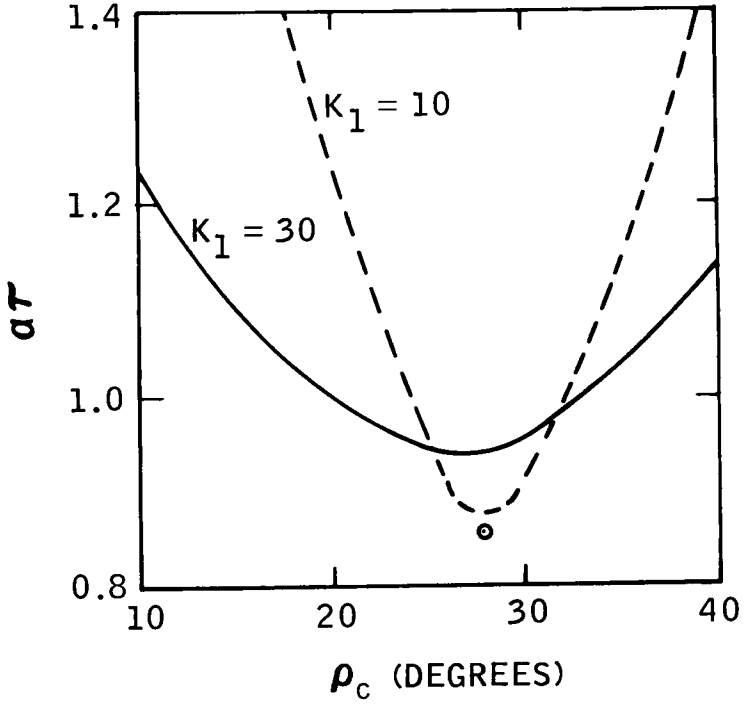

FIGURE 4-7. CHARACTERISTIC VELOCITY AS A FUNCTION OF ρ_c FOR $\phi_{c_0} = 129.2$ DEGREES AND $a = 10^{-3}$

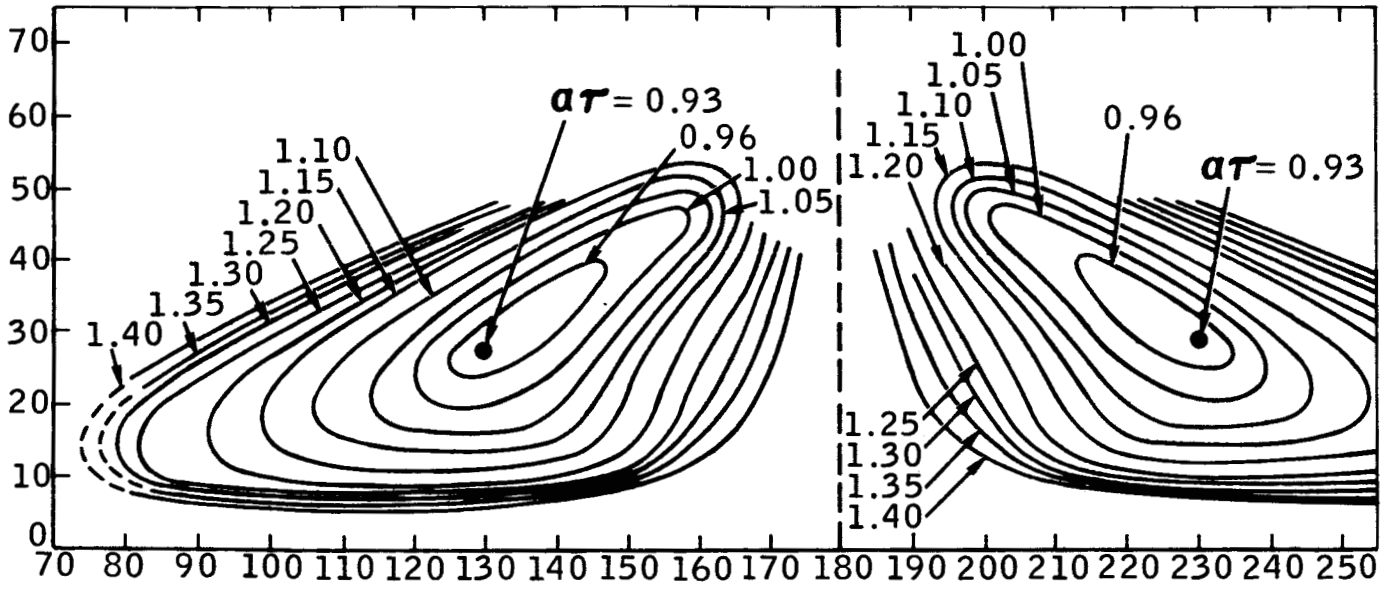

FIGURE 4-8. CHARACTERISTIC VELOCITY CONTOURS AS FUNCTIONS OF THE ORBIT RADIUS AND VELOCITY HEADING ANGLE AT CAPTURE FOR $a = 10^{-3}$ AND $K_1 = 30$

SECTION 5

PLANET-SUN TRANSITION REGIONS

In this study, as in most others, the attraction of the Sun was ignored during the escape and capture phases; and the planetary attractions were ignored during the interplanetary phase. The divison of the problem into three phases is not as clean as one might wish since there are transition regions where the planetary and solar attractions are of the same order. The problem of projecting errors through a transition region using a specified steering law is, in our estimation, the most important unsolved guidance problem for low thrust interplanetary transfer.

For example, the interplanetary phase described in Section 2 terminates when the vehicle arrives at a massless target planet with zero relative velocity. Call this condition A. The capture phase commences when the vehicle achieves zero energy relative to the planet with the planet mass included. Call this condition B. It is not obvious that condition B is ever satisfied by steering to meet condition A. It may be that the terminal guidance scheme, described in Paragraph 4.3, should be initiated before condition A or B is met. Then, too, there is the possibility that capture will be achieved too far from the planet; in which case, the vehicle stops at some point where the thrust acceleration exceeds the planet attraction.

The rotating xy coordinate frame used in Paragraph 2.5 is ideally suited for describing the motion in a transition region. Adding the attraction of the planet P_i to (2-19), one obtains

$$\ddot{x} - 2n\dot{y} - 3n^2 x + \frac{km_i\, x}{\left(|x^2 + y^2|\right)^{3/2}} = f \cos \psi^* \qquad (5\text{-}1)$$

$$\ddot{y} + 2n\dot{x} + \frac{km_i\, y}{\left(|x^2 + y^2|\right)^{3/2}} = f \sin \psi^*$$

where m_i is the mass of P_i. The function

$$H = \frac{1}{2}(\dot{x}^2 + \dot{y}^2) - \frac{3}{2} n^2 x^2 + \frac{km_i}{\left(|x^2 + y^2|\right)^{1/2}} \qquad (5\text{-}2)$$

is a constant when f is zero, in which case (5-2) defines the JACOBIAN energy integral.

The transition from the interplanetary phase to the capture phase was evaluated for one case using (5-1). The thrust acceleration $\alpha = fr_i^2$ was 0.225 where r_i is the radial distance from the Sun to P_i. The trajectory is shown in Figure 5-1. The initial conditions were such that the vehicle would arrive at P_i with zero velocity if m_i were zero and ψ^* were $\pi/2$. The trajectory shape is almost identical when the planet mass is included, but the time to reach the planet is shorter. The terminal guidance scheme, with $K_1 = 30$ and ξ replaced by H as defined in (5-2), was initiated at $\eta = 0.012$. Using the terminal guidance scheme, the thrust is in the negative tangential direction prior to capture. This, together with the solar perturbation term $3n^2x$, explains why the trajectory bends to the left. Capture occurs inside the circle of equal thrust and gravity acceleration. Consequently, the terminal guidance scheme is capable of circularizing the orbit as shown in Figure 5-2. The dashed lines shown in Figure 5-1 are the locus of points where the solar force $3n^2x$ is equal to the planet force $km_i (x^2 + y^2)^{-1}$.

The successful maneuver shown in Figures 5-1 and 5-2 was more or less accidental. Had the terminal guidance scheme been initiated much earlier or later, convergence to the desired terminal conditions may not have been achieved. A rational basis for switching from one guidance mode to another is a minimum requirement. Better yet, a steering law should be formulated which achieves a smooth transition from one phase to another.

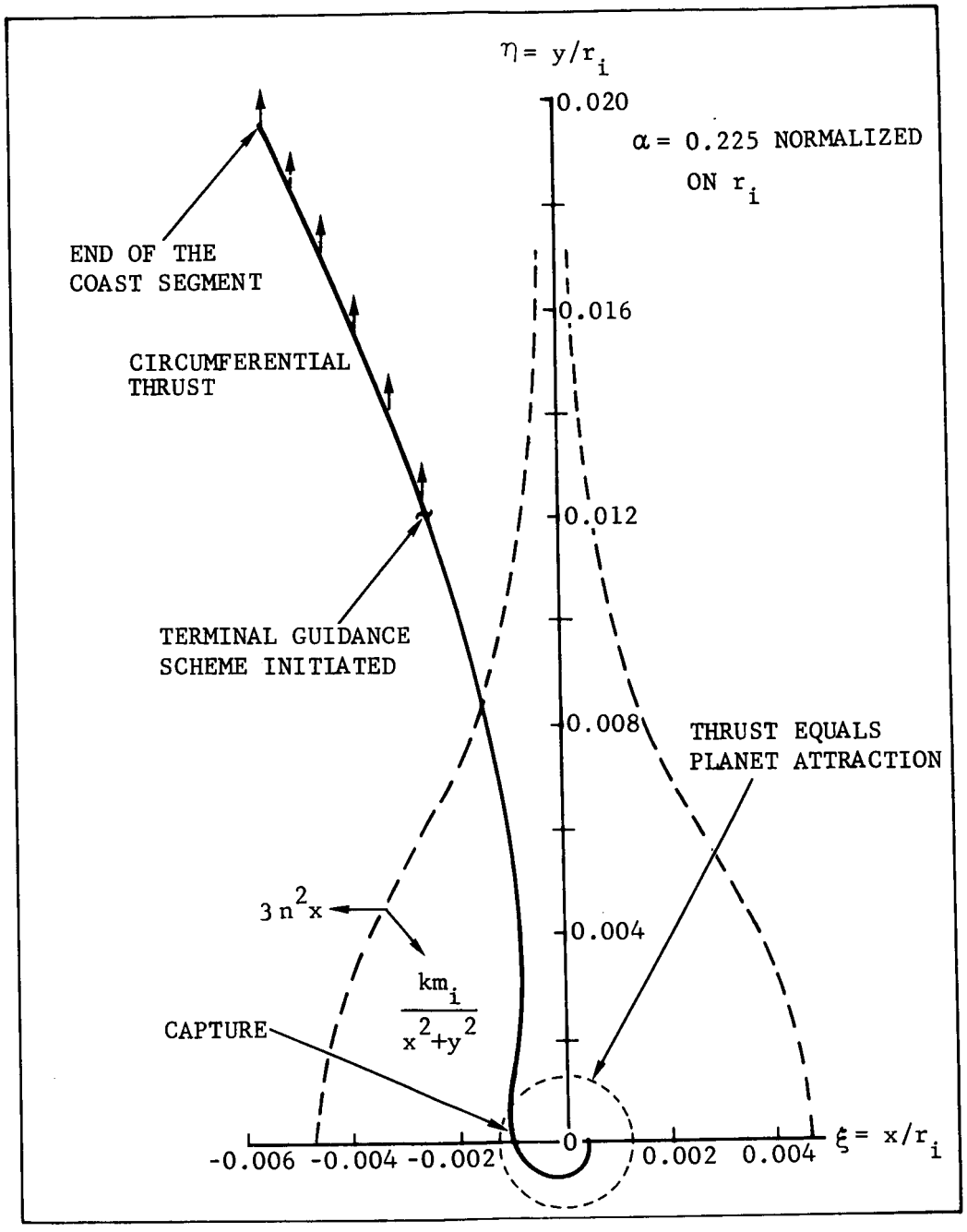

FIGURE 5-1. TRAJECTORY PASSING THROUGH SUN-TARGET PLANET TRANSITION REGION

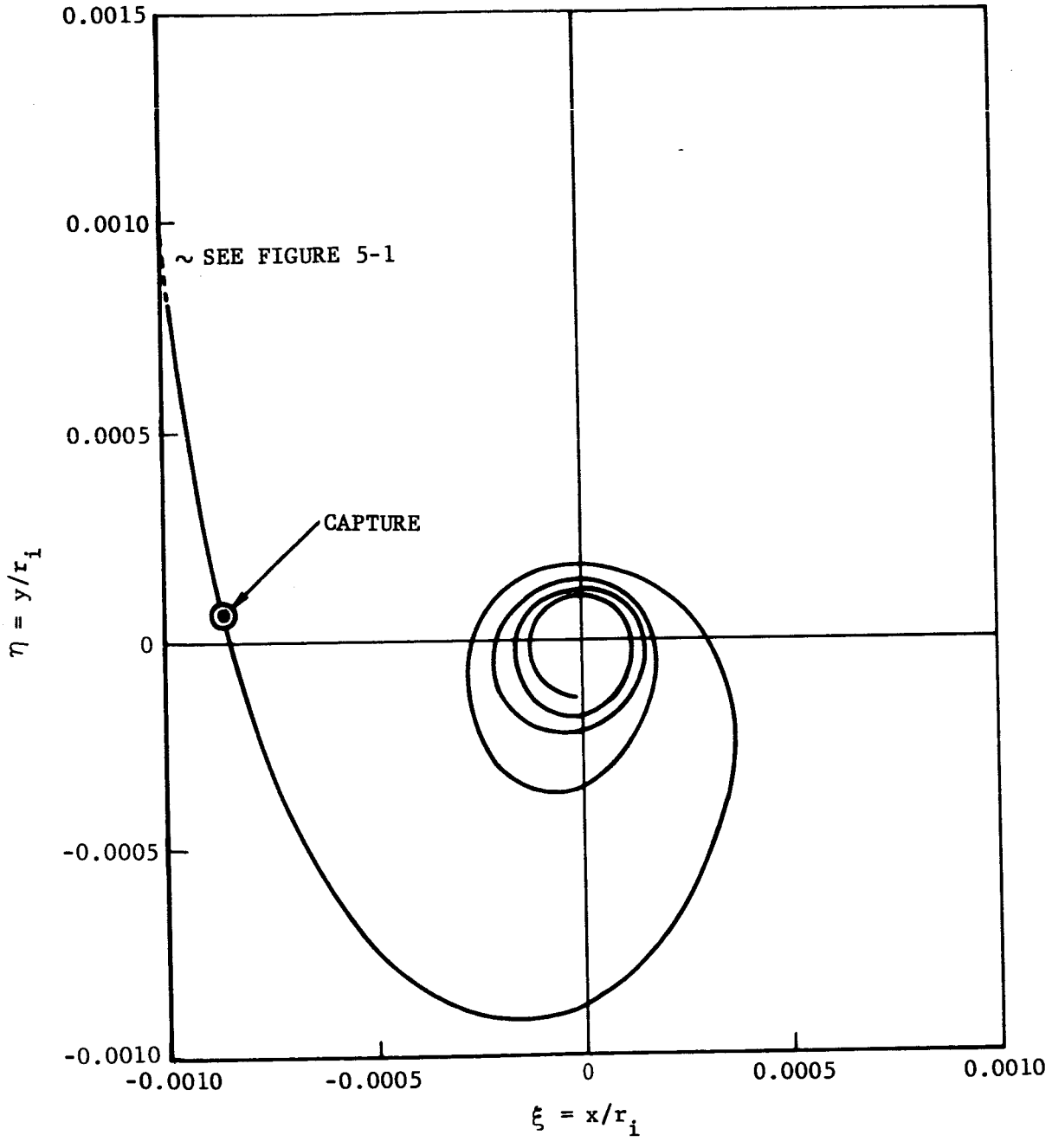

FIGURE 5-2. CAPTURE PHASE USING LINEAR STEERING GAIN, $K_1 = 30$

NOTATION

A	e/w
a	semi-major axis
c	constant proportional to the mass flow rate
E	total energy, $T + V$
$\mathfrak{E}$	normalized total energy
e	orbit eccentricity
f	thrust acceleration
H	JACOBIAN energy integral
h	angular momentum
k	normalized angular momentum
k	universal constant of gravitation
L	$T - V$
m	mass
m_i	mass of the ith planet
n	mean orbit rate
p_r	time derivative of r
r	radial distance
r_i	radial distance from the Sun to the ith planet
T	kinetic energy
t	time
u	reciprocal of r
V	potential energy
v	speed
w	angular momentum squared
XY	nonrotating coordinate system with origin at the Sun
xy	rotating coordinate system with origin at the planet
α	normalized thrust acceleration
β	angle between the thrust and velocity vectors
γ	$\theta - \chi$
η	y/r

NOTATION (Continued)

θ	polar coordinate
θ_L	target planet lead angle
ξ	x/r_i
ρ	normalized radial distance
τ	normalized time
τ_E	escape time
τ_p	total powered time in the interplanetary phase
υ	normalized velocity
Φ	direction of the escape asymptote
ϕ	angle between the velocity vector and the radial direction
χ	phase angle
ψ	angle between the thrust vector and the radial direction
ψ_i	fixed values of for the two thrust segments in the interplanetary phase
$\psi *$	angle between the thrust vector and the x axis

REFERENCES

1. RODRIQUEZ, E., "Method for Determining Steering Programs for Low Thrust Interplanetary Vehicles," ARS Journal, October 1959, pp. 783-788.

2. LEVIN, E., "Low-Thrust Transfer Between Circular Orbits," ASME Preprint 59-AV-2, March 1959.

3. FOX, R. H., "Powered Trajectory Studies for Low Thrust Space Vehicles," ARS Journal, January 1961, pp. 28-32.

4. MOECKEL, W. E., "Interplanetary Trajectories for Electrically Propelled Space Vehicles," Astronautica Acta, Vol. VII/FASC 5-6 1961, pp. 430-444.

5. IRVING, J. H., and BLUM, E. K., "Comparative Performance of Ballistic and Low Thrust Vehicles for Flight to Mars," In: Vistas in Astronautics, Pergamon Press, 1959.

6. MELBOURNE, W. G., "Three-Dimensional Optimum Thrust Equations for Power Limited Propulsion Systems," ARS Journal, Vol. 31, No. 12, December 1961, pp. 1723-1728.

7. MELBOURNE, W. G., and SAUER, C. G., Jr., "Optimum Thrust Programs for Power-Limited Propulsion Systems," Astronautica Acta, Vol. VIII/FASC 4, 1962, pp. 205-227.

8. ZIMMERMAN, A. V., MACKAY, J. S., and ROSSA, L. G., "Optimum Low Acceleration Trajectories for Interplanetary Transfers," NASA TN D 1456, January 1963.

9. MELBOURNE, W. G., and SAUER, C. G., Jr., "Constant-Attitude Thrust Program Optimization," AIAA Journal, Vol. 3, No. 8, August 1965, pp. 1428-1431.

REFERENCES (Continued)

10. ANTHONY, M. L., "An Analytical Approach to the Escape Problem for Large Thrust Vehicles," AIAA Preprint No. 65-551, presented at the AIAA Second Annual Meeting, San Francisco, July 1965.

11. Aeronutronic Report U-2659, "An Investgiation for the Implementation of Adaptive Guidance," April 1964.

12. JOHNSON, D. P., and STUMPF, L. W., "Perturbation Solutions for Low-Thrust Rocket Trajectories," AIAA Journal, Vol. 3, No. 10, October 1965, pp. 1934-1936.

13. ZEE, C. H., "Low-Thrust Oscillatory Spiral Trajectory," Astronautica Acta, Vol. IX, No. 3, 1963, pp. 201-207.

14. LASS, H., and LORELL, J., "Low Acceleration Takeoff from a Satellite Orbit," ARS Journal, Vol. 31, No. 1, January 1961, pp. 24-28.

15. BATTIN, R. H., Astronautical Guidance, McGraw-Hill, 1964, Chapter 10.

16. MIELE, A., "Theorem of Image Trajectories in the Earth-Moon Space," Astronautica Acta, Vol. VI, FASC 5, 1960, pp. 225-232.

17. EDELBAUM, T. H., "Propulsion Requirements for Controllable Satellites," ARS Journal, August 1961, pp. 1079-1089.

18. FAULDERS, C. R., "Minimum-Time Steering Programs for Orbital Transfer With Low Thrust Rockets," Astronautica Acta, Vol. VII/FASC 1, 1961, pp. 35-49.

19. TSIEN, H. S., "Take-Off From Satellite Orbit," ARS Journal, Vol. 23, No. 4, July - August 1953, pp. 233-236.

20. BENNY, D. J., "Escape from a Circular Orbit Using Tangential Thrust," Jet Propulsion, Vol. 28, No. 3, March 1958, pp. 167-169.

21. LAWDEN, D. F., "Optimal Escape from a Circular Orbit," Astronautica Acta, Vol. 4, No. 3, 1958, pp. 218-233.

22. PERKINS, F. M., "Flight Mechanics of Low-Thrust Spacecraft," Journal of the Aerospace Sciences, Vol. 26, No. 5, May 1959, pp. 291-297.

23. COPELAND, J., "Interplanetary Trajectories Under Low Thrust Radial Acceleration," ARS Journal, Vol. 29, April 1959, pp. 267-271.

REFERENCES (Continued)

24. KARRENBERG, H. K., "Note on Interplanetary Trajectories Under Low Thrust Radial Acceleration," ARS Journal, Vol. 30, January 1960, pp. 130-131.

25. AU, G., "Corrections for Interplanetary Trajectories Under Low Thrust Radial Acceleration," ARS Journal, Vol. 30, July 1960, p. 708.

26. BOGOLIUBOFF, N. N., and MITROPOTSKY, Y. A., Asymptotic Methods in the Theory of Nonlinear Oscillations, Hindustan Publishing Corporation (India), 1961, pp. 51-55.